HSATII RNA is induced *via* a non-canonical ATM-regulated DNA-damage response pathway and facilitates tumor cell proliferation and movement

Maciej T. Nogalski[a,1] and Thomas Shenk[a]

[a] Department of Molecular Biology, Princeton University, Princeton, NJ 08544-1014, USA

[1] To whom correspondence may be addressed: nogalski@princeton.edu

Classification: Biological Sciences – Cell Biology

Keywords: HSATII, DNA damage response, human cytomegalovirus, breast cancer cells

ABSTRACT

Pericentromeric human satellite II (HSATII) repeats are normally silent, but can be actively transcribed in tumor cells, where increased HSATII copy number is associated with a poor prognosis in colon cancer, and in human cytomegalovirus (HCMV)-infected cells, where the RNA facilitates viral replication. Here, we report that HCMV infection or treatment of ARPE-19 diploid epithelial cells with the DNA-damaging agents, etoposide and zeocin, induced HSATII RNA expression, and a kinase-independent function of ATM was required for the induction. Additionally, various breast cancer cell lines growing in adherent, 2-dimensional cell culture expressed HSATII RNA at different levels, and levels were markedly increased when cells were either infected with HCMV or treated with zeocin. High levels of HSATII RNA expression correlated with enhanced migration of breast cancer cells, and knockdown of HSATII RNA reduced cell migration and the rate of cell proliferation. Our investigation links high expression of HSATII RNA to the DNA damage response, centered on a non-canonical function of ATM, and demonstrates a role for the satellite RNA in tumor cell proliferation and movement.

SIGNIFICANCE

HSATII RNA is associated with cancer progression, immunostimulation and, as we recently reported, it plays an important role in herpesvirus infections. However, the understanding of cellular processes responsible for the expression of HSATII RNA has been limited. Our current investigation identified a non-canonical, ATM kinase-independent DNA-damage response pathway as a common cellular mechanism regulating HSATII RNA induction in virus-infected cells or cells treated with DNA-damaging agents. Additionally, our study provides a link between expression of HSATII RNA and the cellular growth and migration phenotypes of cancer cells, establishing a new paradigm to study the biological consequences of HSATII RNA expression, i.e., treatment of normal diploid and tumor cells with DNA-damaging agents.

52 ## INTRODUCTION

53 Repetitive DNA sequences comprise more than 50% of the human genome (1) and include short
54 (SINE) and long (LINE) interspersed nuclear elements, DNA transposons, long terminal repeat (LTR)
55 transposons and satellite repeats. Even though repetitive DNA elements are ubiquitous in the human
56 genome, there is a relatively limited understanding of their functions and the molecular mechanisms
57 regulating their expression. Satellite DNAs (satDNAs), which account for ~3% of the genome (1), are
58 constituents of centromeric and pericentromeric heterochromatin, and have been implicated in
59 chromosome organization and segregation, kinetochore formation as well as heterochromatin
60 regulation (2). Next-generation sequencing showed these genomic sites, originally thought to be largely
61 transcriptionally inert, can produce non-coding RNAs (ncRNAs), contributing to satDNA functions (3-6).

62 Altered patterns of transcription, including the induction of ncRNA accumulation, occur in tumors (7-9).
63 Several ncRNAs originating from satDNA regions of the genome are expressed in cancer cells, such as
64 human alpha-satellite repeat (Alpha/ALR) RNA, human satellite II (HSATII) RNA and its mouse
65 counterpart GSAT RNA (10-13). While some satDNA transcription is stress-dependent (14) or triggered
66 during apoptotic, differentiation or senescence programs in cells (15, 16), HSATII RNA accumulation
67 was found to be refractory to these generalized stressors. Rather, it was induced in a series of
68 colorectal cancer cells when they were grown under non-adherent conditions or as xenografts in mice
69 (17). High expression of Alpha/ALR and HSATII RNAs can lead to their reverse transcription and stable
70 reintegration into the human genome, expanding their genomic copy numbers (17). Elevated copies of
71 genomic HSATII sequences were found in primary human colon tumors and correlated with lower
72 survival rates of colon cancer patients (17). Additionally, HSATII and GSAT RNAs have a nucleotide
73 motif usage that is distinct from that commonly seen in most non-coding transcripts, resulting in their
74 immunostimulatory potential (18).

75 Viruses de-regulate many biological processes, often in a similar manner to aberrations seen in cancer
76 cells. Those biological changes caused by infections not only resemble cancer, but in some cases
77 contribute to oncogenesis (19). Indeed, it is estimated that 12-20% of all cancers have a viral etiology
78 and often are linked to persistent or chronic viral infections (20-22).

79 Human cytomegalovirus (HCMV) is a β-herpesvirus that infects a large percentage of the adult
80 population worldwide. Infection in immunocompetent people is typically asymptomatic. In contrast,
81 HCMV is a life-threatening opportunistic pathogen in immunosuppressed individuals (23-25), and a
82 major infectious cause of birth defects (26). Many of the biological changes seen in HCMV-infected
83 cells resemble those common to cancers, including activation of pro-oncogenic pathways, changes in
84 cellular metabolism and increased cell survival (27-32). Given similarities in the molecular symptoms of
85 HCMV infections and tumorigenesis, as well as its reliable presence in glioblastoma tumors, HCMV has
86 been suggested to play a role, perhaps an oncomodulatory role, in the etiology of several human

87 cancers (29, 33-39). However, its high prevalence has made it difficult to establish causality in the
88 disease (40).

89 Recently, we determined that HCMV infection induces HSATII RNA in fibroblasts, among other satDNA
90 transcripts, to a similar extent as reported for tumor cells (41). Elevated HSATII RNA was also detected
91 in biopsies of CMV colitis, showing that the RNA is elevated in human infections and raising the
92 possibility that elevated HSATII RNA may influence the pathogenesis of HCMV disease. When the
93 amount of HSATII RNA in HCMV-infected cells was reduced by knockdown (KD) with locked nucleic
94 acid (LNA) oligonucleotides, viral gene expression, DNA accumulation and yield were reduced.
95 Moreover, KD experiments revealed that HSATII RNA affects several infected-cell processes, including
96 protein stability, posttranslational modifications and motility of infected cells.

97 The HCMV IE1 and IE2 proteins induce HSATII RNA in infected cells (41); and are known to regulate
98 the Rb and E2F protein families, which contribute to efficient viral replication in part through induction of
99 a DNA damage response (DDR) (42, 43). Here, we have tested the possibility that these two activities
100 of the viral IE1 and IE2 proteins - induction of a DDR and HSATII RNA - are related. We report that the
101 DNA-damaging agents, zeocin and etoposide, which induce DNA double-strand breaks (DSBs) and a
102 DDR (44, 45), markedly induce HSATII RNA in diploid epithelial cells growing in adherent, 2-
103 dimensional culture. Consistent with this observation, ATM, a key regulator of DDRs, is required for
104 induction of the satellite RNA by infection or DNA-damaging agents. HSATII RNA induction requires a
105 non-canonical, kinase-independent ATM function. Finally, we demonstrate that HSATII RNA is
106 expressed in a variety of breast cancer cell lines grown in adherent culture, the RNA is further induced
107 in these cell lines by HCMV infection or zeocin treatment, and HSATII RNA levels correlate with their
108 migration and proliferation rates. In sum, our data argues that the DDR leads to elevated HSATII RNA
109 levels, potentially enhancing the fitness of both HCMV and tumor cells.
110

111 ## RESULTS

112 **The DDR regulates HSATII RNA expression.** Ectopic expression of the HCMV IE1 and IE2 proteins
113 can induce HSATII RNA expression in the absence of infection (41). As IE1 and IE2 induce a DDR that
114 supports efficient viral replication (42, 43), we speculated that the DDR could play a role in the
115 expression of human satDNAs.

116 To test this hypothesis, ARPE-19 cells were stressed by three regimens that induce a DDR: UV-C
117 irradiation, H_2O_2 treatment or serum withdrawal (46-48). Exposure of these diploid epithelial cells, which
118 normally express HSATII RNAs at very low basal levels, to these stressing agents induced HSATII
119 RNA to a very limited extent, 2-3 fold (Fig. 1*A*), in contrast to the 100-1000-fold induction observed in
120 response to virus infection (41). As a proxy to monitor successful DDR activation, the induction of p53
121 activity was monitored by assaying the levels of p53-dependent cyclin-dependent kinase inhibitor 1

122 (p21; encoded by the CDKN1A gene) (46) and p53-regulated Damage Induced Noncoding (DINO)
123 lncRNA (49). As expected, both were elevated in cells exposed to all three treatments (Fig. 1*A*).

124 We reasoned that the failure of these treatments to induce HSATII RNA might be a consequence of the
125 specific type of DNA damage and the resulting response that they induce. For example, while UV-C
126 irradiation can lead to DNA double-strand brakes (DSBs), the specific role of UV-C in DNA damage
127 depends on the replicative state of treated cells, as those breaks usually arise from the replication of
128 unrepaired UV-induced DNA lesions (50, 51). It was possible that UV-C and the other treatments were
129 not efficient in inducing HSATII RNA. Therefore, we tested the effects of zeocin and etoposide.
130 Etoposide, similarly to doxorubicin, is an anticancer agent that poisons topoisomerase II, stabilizing
131 DNA-protein complexes, which ultimately leads to stalled replication forks (52). Zeocin belongs to the
132 bleomycin/phleomycin-family of antibiotics and, as a radiomimetic, has similar effects on DNA as
133 ionizing radiation (53). Both drugs induce DNA DSBs (44, 45), and etoposide has been shown to
134 stimulate the expression and retrotransposition of another repeated element, mouse B2 SINE RNA (54,
135 55). ARPE-19 cells were exposed to increasing concentrations of zeocin or etoposide and HSATII,
136 CDKN1A and DINO RNA expression were monitored. Zeocin caused a rapid, dose-dependent
137 induction of HSATII RNA, reaching an ~500-fold increase relative to untreated cells, at the maximum
138 dose tested (400 μg/mL) (Fig. 1*B*). Etoposide also elevated HSATII RNA levels, reaching an ~700-fold
139 increase at the highest dose tested (500 μM) (Fig. 1*C*). CDKN1A and DINO RNA expression mirrored
140 HSATII RNA accumulation, reaching a 6-7-fold induction in cells exposed to 400 μg/mL of zeocin (Fig.
141 1*B*) and ~25-fold induction in cells treated with 500 μM of etoposide (Fig. 1*C*). No ARPE-19 cell toxicity
142 was detected at any drug concentration after a 24 h treatment (Figs. 1*B* and *C*).

143 The kinetics of HSATII, CDKN1A and DINO RNA expression were monitored by RT-qPCR from 0-24 h
144 post treatment (hpt) with zeocin (200 μg/mL) or etoposide (200 μM). HSATII RNA expression started to
145 increase between 7-12 hpt with either zeocin or etoposide, reaching a 300-fold induction at 24 hpt
146 compared to solvent control-treated cells (Figs. 1*D* and *E*). The dynamics of CDKN1A and DINO RNA
147 expression were accelerated compared to HSATII RNA expression, as both transcripts reached their
148 maximum levels within the first 2-4 hpt, suggesting a possible decoupling of DDR/p53-dependent
149 pathways from the mechanism regulating HSATII RNA induction.
150

151 **Zeocin treatment substantially mimics the transcriptional effect of HCMV infection on HSATII**
152 **RNA expression.** To compare the induction HSATII RNA by virus versus DNA-damaging agent,
153 ARPE-19 cells were infected with HCMV or treated with zeocin. The infection used an epithelial cell-
154 grown HCMV strain (TB40/E-GFP-epi) that efficiently infects ARPE-19 cells (56). Mock-infection and
155 solvent treatment served as controls. After 24 h, RNA was isolated and analyzed by using RNA-seq. By
156 analyzing only uniquely mapped HSATII reads, RNA-seq analysis confirmed that zeocin effectively

157 induces HSATII expression in ARPE-19 cells (Fig. 2*A*). Moreover, as in HCMV-infected cells (41),
158 HSATII RNA in zeocin-treated cells is produced preferentially from chromosome 1, 2, 10, and 16. We
159 detected a higher prevalence of HSATII-specific reads from chromosome 1 in cells exposed to zeocin
160 (~15%) compared to only ~5% of these reads in samples from HCMV-infected cells (Fig. 2B). However,
161 in both HCMV- or zeocin-treated cells the majority (~86% or 76%, respectively) of HSATII specific
162 reads mapped to chromosome 16 (Fig. 2*B*).

163 Read coverage tracks at the HSATII-rich locus on chromosome 16 were mapped with the Integrative
164 Genomics Viewer (IGV) using STAR aligner (57)-created BAM files (Fig. 2*C*). The data from mock-
165 infected and solvent-treated cells showed very few, if any, reads mapped to this HSATII locus (Fig. 2*C*).
166 The read coverage tracks based on RNA-seq data from HCMV-infected or zeocin-treated ARPE-19
167 cells display a similar distribution in this HSATII–rich locus spanning approximately 17 kb of DNA.
168 Therefore, these data strengthened our view that common mechanisms might be responsible for the
169 induction of HSATII RNA in both HCMV-infected and DNA-damaging drug-treated cells.
170

171 **Zeocin treatment partially mimics the HCMV-induced transcriptome.** To assess common biological
172 processes regulated by infection and drug, ARPE-19 cells were HCMV-infected or zeocin-treated, and,
173 again, mock-infection or solvent treatment served as controls. The RNA-seq analysis determined that
174 654 and 914 cellular RNAs were significantly ($q < 0.05$) modulated in HCMV-infected and zeocin-
175 treated cells, respectively, and 87 RNAs were modulated by both treatments (Fig. 3*A*). The 87 co-
176 regulated genes were further analyzed by Gene Set Enrichment Analysis (GSEA) (58) using the
177 hallmark gene set of the Molecular Signatures Database (MSigDB) (59) and found to be strongly
178 associated with multiple gene subsets related to DNA damage/repair and other processes, which, if
179 deregulated, associate with enhanced cancer progression (60-63) (Fig. 3*B*). As we were interested in
180 determining the common molecular mechanisms that govern HSATII RNA induction in infected and
181 zeocin-treated cells, we focused on the role of HCMV- and drug-induced DDR pathways in HSATII
182 RNA expression and its possible effect on cancer cell biology.
183

184 **ATM is required for HSATII RNA expression.** Different types of DNA damage govern the activation of
185 DDR pathways through key regulators: ATM, ATR and DNA-PKcs (64-66), and each of these PI3-
186 kinases, when activated, phosphorylates the histone H2A family member, H2AX, generating γ-H2AX
187 (67). HCMV infection induces accumulation of γ-H2AX (42, 43) as does zeocin (68). To confirm that
188 both agents induce this marker in ARPE-19 epithelial cells, untreated, HCMV-infected, or zeocin-
189 treated (100 μg/mL) cells were fixed after 24 h, stained with antibody recognizing γ-H2AX protein and
190 representative images were captured. Both HCMV-infected and zeocin-treated cells had elevated γ-
191 H2AX signals (Fig. 4*A*), however, cells exposed to zeocin were characterized by a higher number of γ-

192 H2AX-positive cells (65%) than HCMV-infected cells (14%) at 24 h after infection or drug treatment
193 (Fig. 4*B*).

194 We next scrutinized possible contributions of ATM, ATR and/or DNA-PKcs to HSATII RNA
195 accumulation. ARPE-19 cells were transfected with NT siRNA or siRNAs targeting ATM, ATR or
196 PRKDC (encodes DNA-PKcs) transcripts. 48 h later, the cells were infected with HCMV or treated with
197 zeocin (100 μg/mL) for 24 h. All siRNAs efficiently reduced their targeted transcripts (75-90% decrease)
198 (Fig. 5*A*). However, only ATM-specific siRNA treatment led to a significant reduction of HSATII RNA
199 levels (~70% decrease) in HCMV-infected (Fig. 5*A*, left panel) or zeocin-treated cells (Fig. 5A, right
200 panel). To directly assess the importance of ATM kinase activity (66, 69, 70) in HSATII RNA induction
201 the effect of Ku-55933 or AZ31, ATM kinase inhibitors (71, 72), were tested. Neither drug compromised
202 the viability of ARPE-19 cells when tested at concentrations up to 50 μM (Fig. 5B, left panel). However,
203 because we noticed morphological changes in treated cells at the highest dose (50 μM), we used Ku-
204 55933 and AZ31 at 20 μM, which is in the range of concentrations at which these drugs are typically
205 used (71-73). Cells were pretreated with Ku-55933 or AZ31 for 2 h before being treated with zeocin
206 (100 μg/mL). Interestingly, at 24 hpt neither ATM kinase inhibitor affected HSATII RNA levels (Fig. 5*B*,
207 right panel). However, both kinase inhibitors negatively (~70% decrease) affected expression of
208 CDKN1A and DINO transcripts when compared to DMSO-treated control cells, demonstrating that the
209 drugs were active.

210 To further establish a role for ATM in HSATII RNA expression, we used ataxia-telangiectasia
211 fibroblasts, A-T(-) cells, that carry a missense mutation in the carboxy-terminal PI3-kinase-like domain
212 of ATM, and contain very low levels of mutant protein (74, 75). A derivative of this cell line, A-T(+) cells,
213 with a stably expressed, functional ATM gene (75) was used as a control. Cells were HCMV-infected or
214 treated with zeocin (100 μg/mL). Mock infection and solvent treatment served as controls. After 24 h,
215 infected and drug-treated A-T(+) cells were characterized by a 71x or 137x induction of HSATII RNA,
216 respectively; and zeocin-treated, but not HCMV-infected, cells contained higher levels of CDKN1A and
217 DINO RNA. HSATII RNA was also induced in A-T(-) cells following HCMV infection or zeocin treatment,
218 but to an ~6-fold lower level when compared A-T(+) cells (Fig. 5*C*). Both treatments resulted in
219 significantly lower expression of CDKN1A and DINO RNAs (~15x and ~5x lower, respectively) in A-T(-)
220 cells when compared to A-T(+) cells. Together these data further implicate ATM in HSATII RNA
221 expression following infection or treatment with DNA-damaging drugs.

222 Next, to confirm a kinase-independent role for ATM in HSATII RNA expression, we ectopically
223 expressed wild-type ATM (ATM*wt*), kinase-dead ATM (ATM*mut*) or GFP, as a control, in the A-T(-)
224 fibroblasts and followed with zeocin treatment. As originally demonstrated by Ziv *et al.* A-T(-) fibroblasts
225 are characterized by a very low level of ATM protein (75) and transfection of the cells with ATM-
226 encoding plasmids resulted in the efficient expression of ATM*wt* or ATM*mut* (Fig. 5D, left panel).

227 ATM*wt*- but not ATM*mut*-expressing cells responded to zeocin treatment with enhanced
228 phosphorylation of Chk2 at threonine 68, as predicted. HSATII RNA levels were monitored in these
229 cells. Similarly to the data presented in figure 5*C*, zeocin treatment increased HSATII expression in
230 untransfected or GFP A-T(-) cells (Fig. 5*D*, right panel). Importantly, however, both ATM*wt*- and
231 ATM*mut*-expressing A-T(-) cells responded to zeocin treatment with similarly increased HSATII RNA
232 expression, when compared to untransfected or GFP-expressing cells. This experiment confirms that
233 ATM regulates HSATII expression, but independently from its kinase activity.
234
235 **HSATII RNA expression is induced by ATM *via* a Chk1/2- and p53-independent pathway**. ATM
236 and ATR phosphorylate two downstream kinases, checkpoint 1 and 2 (Chk1 and Chk2 encoded by the
237 CHEK1 and CHEK2 genes, respectively), which ultimately regulate p53 activity in a context-dependent
238 manner (66, 69, 70). Chk2 is normally activated by ATM-mediated phosphorylation, so we tested
239 whether it is required for accumulation of HSATII RNA. As a control, we also tested Chk1. 48 h prior to
240 HCMV infection or treatment with zeocin (100 μg/mL), ARPE-19 cells were transfected with NT siRNA
241 or siRNA specifically targeting CHEK1 or CHEK2 transcripts (encoding Chk1 or Chk2, respectively).
242 The treatment resulted in a robust decrease in these transcripts at 24 hpi or 24 hpt (Fig. 6*A*). However,
243 we did not detect a statistically significant decrease of HSATII RNA levels in CHEK1 or CHEK2 KD
244 cells upon HCMV infection or zeocin treatment, consistent with the lack of a requirement for ATM
245 kinase activity (Fig. 5), and further arguing that the canonical ATM-Chk2 signaling cascade does not
246 play an important role in the expression of HSATII RNA.

247 Since ATM (76) and Chk2 (77) both phosphorylate and stabilize/activate p53, we also investigated the
248 possible involvement of p53 in HSATII RNA induction. Control and p53 KD ARPE-19 cells were HCMV-
249 infected or treated with zeocin (100 μg/mL), and HSATII, CDKN1A and DINO RNA expression were
250 assessed at 24 (Fig. 6*B*) and 120 hpi/hpt (Fig. 6*C*). TP53-specific siRNA strongly decreased the
251 targeted p53 transcript at both times tested (~83% and 87%), when compared to NT siRNA-treated
252 cells. p53 KD had a modest effect (10% decrease) on HSATII RNA expression at 120 hpi when
253 compared to control cells, but zeocin treatment either had no effect (24 hpt) or slightly increased
254 HSATII RNA expression (120 hpt). In control experiments, p53 KD had little effect on CDKN1A and
255 DINO expression at 24 h post HCMV infection, but significantly decreased (~65%) both transcripts at
256 120 hpi. In comparison, p53 KD strongly (80% decreased) affected CDKN1A and DINO expression at
257 both 24 and 120 h post zeocin treatment.

258 In sum, ATM protein is required for HSATII RNA accumulation in response to infection or zeocin
259 treatment. However, ATM kinase activity and two downstream elements of the DDR response that are
260 normally activated by ATM-mediated phosphorylation, Chk2 and p53, are not required for HSATII RNA
261 expression.

262

263 **Breast cancer cells differ in HSATII RNA levels and sensitivity to HCMV infection and zeocin**
264 **treatments.** HSATII RNA expression has been detected in several cancers, including breast (10, 12),
265 and HSATII copy number gains are a common and negative prognostic feature of colorectal tumors
266 (17). Given the induction of HSATII RNA by HCMV infection (41) and DNA-damaging agents (Fig. 1),
267 and knowing that deregulated DDRs allow cancer cells to achieve high proliferation rates while making
268 them more susceptible to DNA-damaging agents (53, 78), we explored the consequences of induced
269 HSATII RNA expression in breast cancer cells. Initially, we assessed HSATII RNA expression levels in
270 breast cancer cell lines that differed by p53 status, hormonal dependency and invasiveness (Fig. 7*A*).
271 We tested less invasive tumor cell lines: MDA-MB-175VII (ER+, PR-, HER2-, p53 wt), MDA-MB-361
272 (ER+, PR+/-, HER2-, p53 wt), MCF7 (ER+, PR+, HER2-, p53 wt); more invasive triple negative breast
273 cancer (TNBC) cell lines with mutated p53: SUM1315M02, MDA-MB-231, BT-549; and "normal" MCF-
274 10A breast epithelial cells as well as "normal" diploid ARPE-19 cells (79). Cells were cultured in an
275 adherent, 2-dimensional format using identical media conditions across all lines to prevent variations in
276 results potentially caused by different culture conditions. Upon reaching 80-90% confluency, RNA
277 samples were collected. The basal levels of HSATII RNA in the three less invasive cell lines (MCF-7,
278 MDA-MB-175VII and MDA-MB-361) were 5-6-fold higher when compared to HSATII expression in
279 ARPE-19 cells; and the three more invasive cell lines (SUM1315M02, MDA-MB-231, BT-549) were
280 characterized with 14- to 53-fold higher levels of HSATII RNA compared to less invasive breast cancer
281 cells or ARPE-19 cells. The "normal" MCF-10A breast epithelial cells had HSATII RNA levels similar to
282 the less invasive group of tumor cells, suggesting that the basal level of HSATII RNA might be
283 influenced by the tissue origin of tested cells.

284 Next, we tested the induction of HSATII RNA in a selection of the breast cancer cell lines in response to
285 HCMV infection (Fig. 7*B*). At 48 hpi, all tested cells, except BT-549 cells, demonstrated significantly
286 elevated but varied levels of HSATII RNA (from ~5-fold increase in MCF-7 and MDA-MB-231 to ~100-
287 fold increase in MDA-MB-361 and SUM1315MO$_2$) compared to its levels in uninfected cells. As we
288 previously established that HCMV IE1 and IE2 proteins collaborate to induce HSATII RNA (41) and
289 knowing that HCMV replication is limited or abortive in cancer cells (56, 80, 81), we monitored
290 expression of UL123 and UL122 viral transcripts, encoding the IE1 and IE2 proteins. UL123 and UL122
291 RNA expression was detected in the breast cancer cell lines upon HCMV infection (Fig. 7B). However,
292 our data did not detect any correlation between levels of HSATII RNA and viral transcripts.

293 We also tested the effect of zeocin treatment on HSATII RNA induction in these breast cancer cell lines
294 (Fig. 7*C*). At 24 and 96 hpt, all cell lines responded to zeocin with significantly elevated levels of HSATII
295 RNA compared to its levels in solvent control-treated cells. Additionally, a longer exposure (96 h) of
296 cells to the DNA-damaging drug correlated with even higher expression of HSATII RNA. At 96 hpt

297 HSATII RNA levels increased by as much as 240-fold in the case of MCF-10A cells.
298
299 **DNA damage-induced HSATII RNA enhances motility and proliferation of breast cancer cells.**
300 We previously reported that HSATII RNA KD reduced the motility of HCMV-infected ARPE-19 cells
301 (41). Since HCMV infection and zeocin treatment elevated HSATII RNA expression in breast cancer
302 cell lines (Fig. 7*B* and *C*), we tested whether induced HSATII RNA influences migration of these cells.
303 Infection of breast cancer cells at a high multiplicity with HCMV leads to viral protein expression in only
304 a portion of the cells (56), and this would confound interpretation of the migration assay. Therefore, we
305 treated ARPE-19, MCF-7 and SUM1315MO2 cells with zeocin (200 μg/mL) or H_2O as a solvent control
306 to guarantee a uniform effect across the cell population (Fig. 8*A*). At 24 hpt, transwell migration assays
307 (82) were performed using equal numbers of cells and cell motility was assessed after an additional 24
308 h. ARPE-19 and MCF-7 cells showed an ~ 70% and 100% increase in migration, respectively, upon
309 zeocin treatment when compared to solvent control-treated cells. Interestingly, this phenomenon was
310 not observed with SUM1315MO2 cells. Indeed, zeocin caused a slight decrease in the motility of these
311 cells. Although additional cells must be assayed to reach a firm conclusion, this result raises the
312 possibility that cells with high basal HSATII RNA levels might be less sensitive to zeocin treatment.

313 As MDA-MB-231, BT-549 and SUM1315MO2 cells are highly metastatic (83, 84), we tested effects of
314 HSATII RNA KD on the migratory abilities of these three TNBC cells using transwell migration and
315 wound healing (85) assays. For the transwell migration assay, MDA-MB-231, BT-549 and
316 SUM1315MO2 cells were transfected with either NT-LNA or HSATII-LNAs and motility was assessed
317 24 h later (Fig. 8*B*). HSATII-deficient MDA-MB-231, BT-549 and SUM1315 cells exhibited significantly
318 reduced migration relative to control-treated cells. MDA-MB-231 and BT-549 cells were the most
319 sensitive to the treatment with HSATII-LNAs, exhibiting 20- and 5-fold decreases in mean migration,
320 respectively. The wound healing assay provided consistent results (Fig. 8*C*). HSATII-deficient MDA-
321 MB-231, BT-549 and SUM1315 cells were significantly slower in closing wounds compared to control
322 treated cells.

323 As the aggressiveness of TNBC cells is also related to their high proliferation rates, we tested the
324 effects of HSATII KD on the proliferation of MDA-MB-231, BT-549 and SUM1315MO2 cells (Fig. 8*D*).
325 MDA-MB-231, BT-549 and SUM1315MO2 cells were transfected with either NT-LNA or HSATII-LNAs
326 and 24 h later equal numbers of cells were seeded in 2-dimensional cultures and cell proliferation
327 monitored for 5 consecutive days. Although the cell lines proliferated at different rates, the growth rate
328 was significantly reduced for each cell line following HSATII KD.

329 Our data suggest that HSATII RNA is an important regulator linking a DDR with processes involved in
330 cancer cell migration and proliferation. Further, at least some DNA-damaging cancer therapeutics,
331 through the induction of HSATII RNA, might enhance the migration and proliferation of tumor cells.

332

333 ## DISCUSSION

334 Given the ability of HCMV IE1 and 2 proteins to induce a DDR (42, 43) and HSATII RNA (41), and
335 knowing that DNA damage-inducing treatments stimulate the expression of SINEs (54, 55), we tested
336 the possibility that a chemically-induced DDR can also induce HSATII RNA. Zeocin and etoposide
337 robustly induced HSATII RNA in diploid ARPE-19 epithelial cells (Figs. 1*B*) with kinetics (Figs. 1*C*)
338 similar to those described previously for the induction of the transcript by HCMV infection (41). In
339 contrast, UV-C did not induce HSATII (Fig. 1*A*). UV-C causes helix-distorting lesions in DNA, such as
340 pyrimidine(6-4)pyrimidone photoproducts and cyclobutane pyrimidine dimers (50), that can
341 subsequently be converted into DSBs during DNA replication; whereas zeocin (86), etoposide (87) and
342 HCMV infection (88) directly induce DSBs. Our UV-C assay employed confluent monolayers of cells,
343 conditions that did not favor cellular DNA replication and induction of DSBs, so it is possible that
344 extensive DNA DSBs were not produced during the course of the experiment.

345 Zeocin induced expression from a similar set of HSATII loci as did HCMV-infection (Fig. 2*B* and *C*), and
346 a subset of genes induced by zeocin and virus infection overlapped and included key elements of DDR
347 signaling cascades. Infection and zeocin treatment induced γ-H2AX foci in diploid epithelial cells, a
348 marker for DSBs (Fig. 4). The ATM kinase is the primary mediator of the response to DSBs (89), and
349 KD of ATM in diploid epithelial cells (Fig. 5*A* and *B*) blocked HSATII RNA induction by the DNA-
350 damaging drugs and infection. Zeocin, etoposide and virus infection each induce a DDR and HSATII
351 RNA, and these responses depend on ATM. However, although ATM protein is clearly required, two
352 different active ATM kinase inhibitors (Ku-55933 and AZ31) failed to block HSATII RNA induction by
353 zeocin (Fig. 5*B*). Moreover, ectopic expression of wild-type ATM or kinase dead ATM restored the
354 ability of ATM-deficient ataxia-telangiectasia A-T(-) cells to efficiently induce HSATII RNA in response
355 to zeocin treatment (Fig. 5*D*). Further, KD of Chk2, which is activated by ATM-mediated
356 phosphorylation, and KD of p53, which is phosphorylated and activated by both ATM and Chk2, had no
357 effect on HSATII RNA induction by zeocin (Fig. 6*A* and *B*). Thus, our data indicate that ATM kinase
358 activity and the canonical ATM-Chk2-p53 signaling cascade are not required for HSATII RNA
359 accumulation. Different signaling events fit with the observation that the ATM kinase-dependent
360 induction of CDKN1A and DINO RNAs occurs much more rapidly than the ATM kinase-independent
361 induction of HSATII in response to zeocin (Fig. 1*D*) or etoposide (Fig. 1*E*).

362 Even though its kinase activity is not essential, ATM protein (or mRNA) is clearly required for HSATII
363 RNA induction. There is precedent for ATM kinase-independent function. ATM controls mitophagy
364 through its interaction with the Parkin E3 ubiquitin ligase; ATM acts via the protein-protein interaction,
365 independently of its kinase activity (90). We anticipate that the kinase-independent role of ATM in the
366 induction of HSATII RNA might be driven by a similar mechanism.

367 Overexpression of HSATII RNA has been reported for lung, ovarian, prostate and osteosarcoma
368 tumors as well as tumor-derived cell lines (10, 12, 13). Given our current data revealing the importance
369 of the DDR in HSATII RNA expression and with the known impact of deregulated DDRs and cell cycle
370 checkpoints on oncogenesis (91, 92), we probed the physiological consequences of HSATII RNA
371 expression in cultured tumor cells. We tested several breast cancer cell lines growing in adherent, 2-
372 dimensional culture, and higher endogenous HSATII RNA levels correlated with a highly metastatic
373 phenotype (Fig. 7*A*), and HSATII levels were substantially increased in most cell lines by HCMV
374 infection or zeocin treatment (Fig. 7*B* and *C*). Cells characterized by low basal HSATII RNA expression,
375 i.e. ARPE-19 and MCF-7 cells, showed an enhanced migratory phenotype when exposed to zeocin,
376 while SUM1315MO2 cells with higher uninduced levels of HSATII RNA did not (Fig. 8*A*). Perhaps the
377 non-responsive cells had a sufficiently high level of the satellite RNA before induction. HSATII RNA KD
378 markedly reduced migration (Fig. 8*B* and *C*) and proliferation (Fig. 8*D*) in the three TNBC cell lines
379 tested, suggesting a direct relationship between high levels of the RNA and cell phenotype. These
380 observations argue that higher HSAII RNA levels correlate with enhanced proliferation and migration,
381 characteristics of aggressive, metastatic tumors; and they are consistent with an earlier report showing
382 that HSATII copy number gains are a negative prognostic feature of colorectal cancers (17).

383 DNA-damaging cancer therapeutics can lead to drug resistance (53, 78) and raise concerns about the
384 development of *de novo* primary tumors (93). The induction of HSATII RNA accumulation by DNA-
385 damaging drugs in cultured cells (Fig 1 and 7) and the correlation between elevated HSATII RNA and
386 enhanced tumor cell proliferation and migration (Fig. 8) prompts us to speculate that DNA-damaging
387 chemotherapeutics have potential to enhance malignancy of tumor cells that survive treatment. This
388 effect could be of long or short duration, depending on how long HSATII RNA remains elevated after
389 drug treatment. Negative consequences could derive from immediate effects of HSATII RNA
390 overexpression, as we have measured here, and perhaps overexpression of other non-coding RNAs. In
391 addition, longer-term effects might result from reverse transcription of the overexpressed RNAs
392 followed by integration and copy number expansion in tumors, as described for HSATII (17) and
393 another repeated element, LINE-1 (94).

394 HCMV RNAs and proteins are found in a variety of human malignancies, and HCMV-infected cells have
395 many properties suggesting the virus might influence tumor progression (95). The ability of HCMV
396 infection, like radiomimetic drugs, to sponsor a DDR (43, 96) with induction of HSATII RNA in healthy
397 cells (41) (Figs. 1 and 2) and breast cancer cells (Fig. 7*B*) leads to a second speculation. Perhaps
398 HSATII RNA induction contributes to the apparent oncomodulatory activity of the virus. Indeed,
399 numerous viruses, many of which are considered tumor viruses, are known to induce a DDR (42); and,
400 therefore, might also induce HSATII RNA contributing to malignancy. For HCMV, even a limited or

401 abortive viral replication documented in cancer cells (56, 80, 81) might lead, *via* IE1/IE2 protein-
402 mediated HSAII RNA induction, to enhanced migratory and proliferative characteristics of cancer cells.

403 In sum, this study demonstrates that DNA DSBs induce HSATII RNA via a DDR that requires ATM
404 protein but not its kinase activity, demonstrates a link between expression of the RNA and cellular
405 growth and migration phenotype, and establishes a new paradigm to study the biological consequences
406 of HSATII RNA expression - treatment of normal diploid and tumor cells with DNA-damaging agents.
407

408 ## METHODS AND MATERIALS

409 **Cells, viruses and drugs.** Human retinal pigment epithelial (ARPE-19) cells, human foreskin
410 fibroblasts (HFFs) (30) and breast epithelial (MCF-10A) cells as well as breast cancer cell lines: MCF-7,
411 MDA-MB-175VII, MDA-MB-361, and MDA-MB-231 were from the American Type Culture Collection
412 (ATCC). SUM1315MO2 breast cancer cells (97) were generously provided by Stephen Ethier (Medical
413 University of South Carolina). A-T(-) fibroblasts, originally named AT22IJE-T, and A-T(+) fibroblasts
414 with a stably expressed functional ATM were created by the lab of Yosef Shiloh (Sackler School of
415 Medicine) (74, 75) and generously provided by Matthew Weitzman (Perelman School of Medicine
416 University of Pennsylvania). ARPE-19, MCF-7, MDA-MB-175VII, MDA-MB-361, MDA-MB-231 and
417 SUM1315MO2 cells were cultured in 10% FBS/DMEM with added Ham's F-12 nutrient mixture (Sigma-
418 Aldrich) and supplemented with 1x MEM Non-Essential Amino Acids Solution (ThermoFisher
419 Scientific), 1 mM sodium pyruvate, 1x GlutaMAX and 10 mM Hepes, pH 7.4. HFFs, A-T(-) and A-T(+)
420 cells were cultured in 10% FBS/DMEM. Media were supplemented with penicillin G sodium salt (100
421 units/ml) and streptomycin sulfate (95 units/ml). IE1 and IE2-expressing ARPE-19 cells were described
422 previously (41).

423 An infectious BAC clone of HCMV strain TB40/E-GFP (TB40/Ewt-GFP) (98) was electroporated into
424 ARPE-19 cells or HFFs to generate viral progeny that were passaged once more in ARPE-19 cells or
425 HFFs, respectively. TB40/E-GFP-epi designates TB40/E-GFP virus grown in ARPE-19 cells (99). All
426 viral stocks were partially purified by centrifugation through a 20% D-sorbitol cushion in buffer
427 containing 50 mM Tris HCl, 1 mM $MgCl_2$, pH 7.2, resuspended in DMEM and stored in aliquots at -
428 80°C. Infections were performed by treating cells with viral inoculum for 2 h, followed by removal of the
429 inoculum and washing with phosphate-buffered saline (PBS; Sigma-Aldrich) before applying fresh
430 medium. To quantify extracellular virions, media from infected cells was collected and spun for 10 min.
431 at 2000 x g to remove debris. To quantify intracellular virions, infected cells were washed with PBS,
432 scrapped and intracellular virus released by 3 rounds of freezing and thawing and then spun for 10 min.
433 at 2000 x g to remove debris. Viral stocks and sample supernatant were titered by plaque assay.

434 Zeocin (InvivoGen) was dissolved in water and stored at -20°C. Etoposide (Millipore Sigma), Ku-55933
435 (Tocris) and AZ31 (Selleckchem) were dissolved in DMSO and stored at -20°C.

436 **RNA sequence analysis (RNA-seq).** RNA was collected in QIAzol Lysis Reagent (Qiagen) and
437 isolated using the miRNeasy Mini Kit (Qiagen). DNA was removed from samples using Turbo DNase
438 (Thermo Fisher Scientific) and RNA quality was assessed using the Bioanalyzer 2100 (Agilent
439 Technologies). Sequencing libraries were prepared using the TruSeq Stranded Total RNA with Ribo-
440 Zero kit (Illumina), and sequenced on Illumina HiSeq2500 sequencer instrument in paired-end, rapid
441 mode (2x 150bp).

442 For RNA-seq analysis, the Galaxy instance of Princeton University was used (100). RNA-Seq data
443 were de-multiplexed based on indexes. Phred quality scores were checked by using the FastQC toolkit
444 and were greater than 26 for more than 90% of the read length. Human and HCMV fasta and
445 annotation (.gtf) files were created for mapping by combining sequences and annotations from Ensembl
446 annotation, build 38 (GRCh38), Repbase elements (release 19) and TB40 (EF999921) when
447 appropriate. Quality filtered reads were mapped to the concatenated human-virus genomes using RNA
448 STAR (57) (Galaxy version 2.6.0b-2). The featureCounts program (101) (Galaxy version 1.6.4) was
449 used to measure gene expression. The resulting files were used as input to determine differential
450 expression for each gene utilizing DESeq2 (102) (Galaxy version 2.11.40.6). Fold changes in gene
451 expression were considered significant when the adjusted *P* value (q value) for multiple testing with the
452 Benjamini–Hochberg procedure, which controls for the False Discovery Rate (FDR), was <0.05.
453 To analyze HSATII expression, aligned reads were assigned using the featureCounts function of
454 Rsubread package (103) with the external HSATII annotation obtained from a RepeatMasker (104)
455 using GRCh38 and Repbase consensus sequences. This produced the raw read counts. HSATII
456 expression in terms of CPM (counts per million reads) was computed and normalized across samples
457 using the trimmed mean of M-values method (TMM) (105). To calculate the percent of HSATII reads
458 originating from each chromosome, we identified uniquely mapped reads that exclusively overlapped
459 with HSATII repeat. The number of normalized counts of HSATII reads mapped to each chromosome
460 was computed and the percentage of these reads mapping to each chromosome was calculated as
461 described previously (41). To visualize read coverage tracks for alignment files, RNA STAR-generated
462 BAM files were imported into the Integrative Genomics Viewer (106) (IGV; version 2.6.3) and aligned
463 with human genome assembly GRCh38 focused on the HSATII locus on chromosome 16. The scale of
464 read coverage peaks was adjusted for experimentally paired samples. To create Venn diagrams, based
465 on data from the DESeq2 analysis the list of significantly expressed genes in HCMV-infected or zeocin-
466 treated cells compared to control cells were imported into a web-based tool InteractiVenn (107).
467 Gene Set Enrichment Analysis (GSEA) (58) was performed on the list of common genes differentially
468 expressed in both HCMV-infected and zeocin-treated cells using the hallmark gene set of the Molecular
469 Signature Database (MSigDB) (59). A matrix of differentially expressed genes from the data set
470 significantly matching the hallmark gene set of MSigDB was composed and a list of the hallmark gene

471 subsets was ordered based on a number of overlapping genes, *p* value determining the probability of
472 association with a given gene set and a FDR q-value.

473 **Quantification of nucleic acids.** For analysis by qRT-PCR, RNA was extracted from samples
474 collected in QIAzol lysis reagent using the miRNeasy kit (Qiagen). cDNA was made from 1 μg of total
475 RNA with random hexamer primers and MultiScribe reverse transcriptase (Applied Biosystems),
476 according to the manufacturer's protocol. Transcript-specific primer sequences used in the study were
477 either previously reported (41) or newly designed: CDKN1A Forward 5'-TTTAACAGCCTGCTCCCTTG-
478 3', Reverse 5'-AGTTTGCAACCATGCACTTG-3'; DINO Forward 5'-GGAGGCAAAAGTCCTGTGTT-3',
479 Reverse 5'-GGGCTCAGAGAAGTCTGGTG-3' (49); E2F1 Forward 5'-CCGTGGACTCTTCGGAGAAC-
480 3', Reverse 5'-ATCCCACCTACGGTCTCCTC-3'; E2F2 Forward 5'-TGGGTAGGCAGGGGAATGTT-3',
481 Reverse 5'-GCCTTGTCCTCAGTCAGGTG-3'; E2F3a Forward 5'-
482 TTTAAACCATCTGAGAGGTACTGATGA-3', Reverse 5'-CGGCCCTCCGGCAA-3' (108); E2F3b
483 Forward 5'-TTTAAACCATCTGAGAGGTACTGATGA-3', Reverse 5'- CCCTTACAGCAGCAGGCAA-3'
484 (108); E2F4 Forward 5'-TGGAAGGTATCGGGCTAAT-3', Reverse 5'-
485 CAATCAGTTTGTCAGCAATCTC-3'; E2F5 Forward 5'-CGGCAGATGACTACAACTTTA-3', Reverse 5'-
486 GATAACAGTCCCAAGTTTCCA-3'; ATM Forward 5'-GCACTGAAAGAGGATCGTAAA-3', Reverse 5'-
487 GAGGGAACAAAGTCGGAATAC-3'; ATR Forward 5'-ATATCACCCAAAAGGCGTCGT-3', Reverse 5'-
488 TGCTCTTTTGGTTCATGTCCAC-3'; PRKDC Forward 5'-AAATGGGCCAGAAGATCGCA-3', Reverse
489 5'-AGGTCCAGGGCTGGAATTTT-3'; CHEK1 Forward 5'-TTTGGACTTCTCTCCAGTAAAC-3', Reverse
490 5'-GCTGGTATCCCATAAGGAAAG-3'; CHEK2 Forward 5'-CGCGGTCGTGATGTCTCGGG-3',
491 Reverse 5'-CGCTGCCATGGGGCTGTGAA-3'; TP53 Forward 5'-AGGGATGTTTGGGAGATGTAAG-3',
492 Reverse 5'-CCTGGTTAGTACGGTGAAGTG-3' (109). qPCR was performed using SYBR Green master
493 mix (Applied Biosystems) on a QuantStudio™ 6 Flex Real-Time PCR System (Applied Biosystems).
494 Transcript levels were analyzed using the delta delta Ct method and GAPDH was used as an internal
495 control (110). Error ranges are reported as standard deviation of the mean (SD).

496 **Analysis of proteins.** For Western blot analysis, transfected A-T(-) were harvested using lysis buffer
497 (50 mM Tris-HCl, pH 7.5, 5 mM EDTA, 100 mM NaCl, 1% Triton X-100, 0.1% SDS, and 10% glycerol).
498 Samples were mixed with 6xSDS sample buffer (325 mM Tris pH 6.8, 6% SDS, 48% glycerol, 0.03%
499 bromophenol blue containing 9% 2-mercaptoethanol). Proteins were separated by electrophoresis
500 (SDS-PAGE) and transferred to ImmunoBlot polyvinylidene difluoride (PVDF) membranes (BioRad
501 Laboratories). Western blot analyses were performed using primary antibodies recognizing ATM
502 (D2E2; Cell Signaling Technology), GFP (D5.1; Cell Signaling Technology), p-Chk2 (T68) (2661; Cell
503 Signaling), Chk2 (2662; Cell Signaling) and β-actin-HRP (Abcam). Donkey anti-rabbit (GE Healthcare
504 Biosciences) conjugated with horseradish peroxidase was used as a secondary antibody. Western
505 blots were developed using WesternSure ECL Detection Reagents (Licor).

506 **Immunofluorescence.** For immunofluorescence assays, ARPE-19 cells grown in 96-well plates were
507 infected with TB40/E-GFP-epi (3 IU/cell), treated with zeocin (200 μg/mL) or left untreated. After 24 h,
508 cells were fixed in 100% methanol (Sigma) and incubated in blocking solution [PBS with 3% bovine
509 serum albumin prior to the addition of a primary mouse monoclonal antibody specific for phospho-
510 Histone H2AX (Ser13; clone JBW301; Millipore Sigma). Following incubation, cells were washed with
511 PBS, and a donkey Alexa488-conjugated anti-mouse secondary antibody (Santa Cruz Biotechnology)
512 was applied. Nuclei were counterstained with the Hoechst stain. Cells were visualized and % of γ-
513 H2AX-positive cells was calculated using the Operetta high-content imaging and analysis system
514 (Perkin Elmer) with 20X objective.

515 **Plasmid transfection.** Plasmids used in the study: pCMV-Neo-Bam was a gift from Bert Vogelstein
516 (Addgene plasmid #16440). pCMV-Neo-Bam E2F3a and pCMV-Neo-Bam E2F3b were gifts from
517 Jacqueline Lees (Addgene plasmid #37970 and #37970, respectively). pCMVHA E2F1 and pCMVHA
518 E2F2 were gifts from Kristian Helin (Addgene plasmids #24225 and #24226, respectively).
519 ARPE-19 cells at 70-80% confluency were transfected with 1 μg of each plasmid using Lipofectamine
520 3000 (Thermo Fischer Scientific) according to the manufacturer's instructions. 72 h later, plasmid-
521 transfected cells were harvested using TRIzol and samples were stored at -80°C.

522 **Cell stress induction.** For the induction of stress by serum deprivation (111), cells were washed with
523 1xPBS, fed with medium lacking FBS and cultured for 24 h. For the oxidative stress (112), cells were
524 washed with 1xPBS, fed with medium lacking FBS, but containing 100 μM of H_2O_2 and cultured for 24
525 h. For UV-irradiation-based stress (113), cells were washed with 1xPBS, exposed to the ultra violet light
526 (50 J/m^2) using a Stratalinker (Stratagene), washed with 1xPBS, supplemented with 10%FBS/DMEM
527 and cultured for 24 h.

528 **Locked nucleic acid and siRNA KD.** Locked nucleic acid (LNA™; Exiqon, Skelstedt, Denmark)
529 oligonucleotides targeting HSATII RNA were described previously (41). Control NT-LNA or HSATII-
530 LNAs (100-200 nM) were transfected into cells using Lipofectamine RNAiMAX® Reagent (Thermo
531 Fisher Scientific) according to the manufacturer's instructions. LNA-treated ARPE-19 cells were
532 incubated for 24-48 h before being subjected to subsequent experimental procedures.

533 siRNAs targeting E2F1 (E2F1 siRNA), E2F2 (E2F2 siRNA), E2F3 (E2F3 siRNA),
534 E2F4 (E2F4 siRNA), E2F5 (E2F5 siRNA), CHEK1 (CHEK1 siRNA) and CHEK2 (CHEK2 siRNA) were
535 siGENOME SMARTpools (Dharmacon). siRNAs targeting ATM (ATM siRNA), ATR (ATR siRNA),
536 PRKDC (PRKDC siRNA) and TP53 (TP53 siRNA) were ON-TARGETplus SMARTpools (Dharmacon).
537 All siRNAs and appropriate NT siRNAs (siGENOME Non-targeting siRNA Pool #1 and ON-
538 TARGETplus Non-targeting Control Pool; Dharmacon) were purchased from Life Technologies. ARPE-
539 19 cells were grown to ~80% confluence and then transfected with siRNA using Lipofectamine®

540 RNAiMAX Reagent (Life Technologies). Cells transfected with non-specific, scrambled siRNA (NT
541 siRNA) (Life Technologies) served as a negative control. Following 48 h incubation with siRNA, cells
542 were washed with 1xPBS and subjected to subsequent experimental procedures.

543 **Cell migration, proliferation and toxicity assays.** Wound healing and transwell migration assays
544 were performed as described previously (41). For wound healing assays, confluent monolayers of NT-
545 LNA- or HSATII-LNA-transfected MDA-MB-231, BT-549 and SUM1315MO2 cells were scratched with a
546 1-ml pipet to create wounds. The process of wound closure was monitored in time using a Nikon
547 Eclipse TE2000-U inverted microscope. The average wound width (in arbitrary units) of ARPE-19 cells
548 was calculated from 6 measurements for each experimental arm from the captured images using
549 ImageJ software (114). Results are plotted as a mean percent of remaining wound width (SD). For
550 transwell assays, NT-LNA- or HSATII-LNA -transfected MDA-MB-231, BT-549 and SUM1315MO2 or
551 zeocin-treated ARPE-19, MCF-7 and SUM1315MO2 cells were trypsinized and 50,000 cells were
552 seeded onto each filter in FBS-free medium containing ITS Liquid Media Supplement (Sigma-Aldrich).
553 After 24 h, filters were washed, cells were fixed and migrated cells on the bottom surface of the filter
554 were stained with 0.2% crytal violet solution. Migrated cells were imaged and quantified using ImageJ
555 software (114).

556 To monitor proliferation, cells were transfected with NT-LNA or HSATII-LNAs. After 48 hpt, equal
557 number of cells (2500 cells/well) were seeded into 96-well plates and cultured in 10% FBS/DMEM with
558 added Ham's F-12 nutrient mixture and supplemented with 1x MEM Non-Essential Amino Acids
559 Solution, 1 mM sodium pyruvate, 1x GlutaMAX and 10 mM Hepes. Cell numbers were quantified using
560 a colorimetric 3-(4,5-dimethylthiazol-2-yl)-5-(3-carboxymethoxyphenyl)-2-(4-sulfophenyl)-2H-
561 tetrazolium (MTS)-based CellTiter 96® AQ_{ueous} One Solution Cell Proliferation Assay (Promega,
562 Madison, WI) according to the manufacturer's protocol. Absorbance was measured at 490 nm using the
563 SpectraMax Plus 384 Microplate reader (Molecular Devices).

564 To assay toxicity, ARPE-19 cells were treated with zeocin, etoposide, Ku-55933 or AZ31 at specified
565 concentrations for 24 h or with water or DMSO as solvent controls. Each tested concentration of a
566 specific drug contained the same concentration of solvent. At indicated times, the CellTiter 96® AQ_{ueous}
567 One Solution Cell Proliferation Assay (Promega) was performed according to the manufacturer's
568 instructions. Absorbance was measured at 490 nm using the SpectraMax Plus 384 Microplate reader
569 (Molecular Devices).

570 **Statistical analysis.** To determine statistical significance between two conditions in experiments,
571 unpaired, two-tailed *t*-tests with Welch`s correction were performed, otherwise one-way ANOVA was
572 performed between the arrays of data from distinct samples to determine *P* values. *P* value <0.05 was
573 considered significant. Significance is shown by the presence of asterisks above data points with one,
574 two, three or four asterisks representing *P*<0.05, *P*<0.01, *P*<0.001 or P<0.0001, respectively. Only

575 significant *P* values are reported.

576 **Data availability.** Raw RNA-seq data will be available from the NCBI Gene Expression Omnibus
577 (GEO). All relevant experimental data are available from the authors.

ACKNOWLEDGMENTS

We thank Stephen Ethier (Medical University of South Carolina) for generously providing SUM1315MO2 cells; Matthew Weitzman (Perelman School of Medicine, University of Pennsylvania) for generously providing A-T(-) and A-T(+) fibroblasts, Adam Oberstein (University of Illinois) for creating IE1/IE2-expressing ARPE-19 cells, Alexander Solovyov (Memorial Sloan Kettering Cancer Center) for advice and assistance with RNA-seq analyses and members of the T.S. laboratory for scientific discussions.

This work was supported by National Institutes of Health Grants AI112951 and AI142520. M.T.N. was partially supported by American Cancer Society Fellowship PF-14-116-01-MPC.

AUTHOR CONTRIBUTIONS

M.T.N. designed and performed experiments, analyzed the data and wrote the manuscript. T.S. supervised the study, analyzed the data and edited the manuscript.

DECLARATION OF INTEREST

Icahn School of Medicine at Mt. Sinai and Princeton University have submitted a provisional patent application based on the use of HSATII-specific LNAs for HSATII knockdown, and M.T.N. and T.S. are co-inventors.

599 **REFERENCES**
600

601 1. A. J. Levine, D. T. Ting, B. D. Greenbaum, P53 and the defenses against genome instability
602 caused by transposons and repetitive elements. *Bioessays* **38**, 508-513 (2016).
603 2. Z. Pezer, J. Brajkovic, I. Feliciello, D. Ugarkovc, Satellite DNA-mediated effects on genome
604 regulation. *Genome Dyn.* **7**, 153-169 (2012).
605 3. A. Eymery *et al.*, A transcriptomic analysis of human centromeric and pericentric sequences in
606 normal and tumor cells. *Nucleic Acids Res.* **37**, 6340-6354 (2009).
607 4. L. E. Hall, S. E. Mitchell, R. J. O'Neill, Pericentric and centromeric transcription: a perfect
608 balance required. *Chromosome Res.* **20**, 535-546 (2012).
609 5. M. A. Garrido-Ramos, Satellite DNA: An Evolving Topic. *Genes (Basel)* **8** (2017).
610 6. S. Louzada *et al.*, Decoding the Role of Satellite DNA in Genome Architecture and Plasticity-An
611 Evolutionary and Clinical Affair. *Genes (Basel)* **11** (2020).
612 7. K. Gronbaek, C. Hother, P. A. Jones, Epigenetic changes in cancer. *APMIS* **115**, 1039-1059
613 (2007).
614 8. R. Kanwal, S. Gupta, Epigenetic modifications in cancer. *Clin. Genet.* **81**, 303-311 (2012).
615 9. A. Sanchez Calle, Y. Kawamura, Y. Yamamoto, F. Takeshita, T. Ochiya, Emerging roles of long
616 non-coding RNA in cancer. *Cancer Sci.* **109**, 2093-2100 (2018).
617 10. D. T. Ting *et al.*, Aberrant overexpression of satellite repeats in pancreatic and other epithelial
618 cancers. *Science* **331**, 593-596 (2011).
619 11. K. I. Leonova *et al.*, p53 cooperates with DNA methylation and a suicidal interferon response to
620 maintain epigenetic silencing of repeats and noncoding RNAs. *Proc. Natl. Acad. Sci. U.S.A.*
621 **110**, E89-98 (2013).
622 12. L. L. Hall *et al.*, Demethylated HSATII DNA and HSATII RNA Foci Sequester PRC1 and MeCP2
623 into Cancer-Specific Nuclear Bodies. *Cell Rep.* **18**, 2943-2956 (2017).
624 13. X. D. Ho *et al.*, Analysis of the Expression of Repetitive DNA Elements in Osteosarcoma. *Front.*
625 *Genet.* **8**, 193 (2017).
626 14. R. Valgardsdottir *et al.*, Transcription of Satellite III non-coding RNAs is a general stress
627 response in human cells. *Nucleic Acids Res.* **36**, 423-434 (2008).
628 15. H. Bouzinba-Segard, A. Guais, C. Francastel, Accumulation of small murine minor satellite
629 transcripts leads to impaired centromeric architecture and function. *Proc. Natl. Acad. Sci. U.S.A.*
630 **103**, 8709-8714 (2006).
631 16. M. De Cecco *et al.*, Genomes of replicatively senescent cells undergo global epigenetic
632 changes leading to gene silencing and activation of transposable elements. *Aging Cell* **12**, 247-
633 256 (2013).
634 17. F. Bersani *et al.*, Pericentromeric satellite repeat expansions through RNA-derived DNA
635 intermediates in cancer. *Proc. Natl. Acad. Sci. U.S.A.* **112**, 15148-15153 (2015).
636 18. A. Tanne *et al.*, Distinguishing the immunostimulatory properties of noncoding RNAs expressed
637 in cancer cells. *Proc. Natl. Acad. Sci. U.S.A.* **112**, 15154-15159 (2015).
638 19. N. A. Krump, J. You, Molecular mechanisms of viral oncogenesis in humans. *Nat. Rev.*
639 *Microbiol.* **16**, 684-698 (2018).
640 20. E. A. Mesri, M. A. Feitelson, K. Munger, Human viral oncogenesis: a cancer hallmarks analysis.
641 *Cell Host Microbe* **15**, 266-282 (2014).
642 21. M. E. McLaughlin-Drubin, K. Munger, Viruses associated with human cancer. *Biochim. Biophys.*
643 *Acta* **1782**, 127-150 (2008).
644 22. M. K. White, J. S. Pagano, K. Khalili, Viruses and human cancers: a long road of discovery of
645 molecular paradigms. *Clin. Microbiol. Rev.* **27**, 463-481 (2014).
646 23. I. G. Sia, R. Patel, New strategies for prevention and therapy of cytomegalovirus infection and
647 disease in solid-organ transplant recipients. *Clin. Microbiol. Rev.* **13**, 83-121, table of contents
648 (2000).
649 24. S. S. Kanj, A. I. Sharara, P. A. Clavien, J. D. Hamilton, Cytomegalovirus infection following liver
650 transplantation: review of the literature. *Clin. Infect. Dis.* **22**, 537-549 (1996).

651 25. G. Gerna *et al.*, Human cytomegalovirus end-organ disease is associated with high or low
652 systemic viral load in preemptively treated solid-organ transplant recipients. *New Microbiol.* **35**,
653 279-287 (2012).
654 26. T. M. Lanzieri, S. C. Dollard, S. R. Bialek, S. D. Grosse, Systematic review of the birth
655 prevalence of congenital cytomegalovirus infection in developing countries. *Int. J. Infect. Dis.* **22**,
656 44-48 (2014).
657 27. M. Michaelis, H. W. Doerr, J. Cinatl, The story of human cytomegalovirus and cancer:
658 increasing evidence and open questions. *Neoplasia* **11**, 1-9 (2009).
659 28. G. Herbein, The Human Cytomegalovirus, from Oncomodulation to Oncogenesis. *Viruses* **10**
660 (2018).
661 29. Q. Lepiller, K. Aziz Khan, V. Di Martino, G. Herbein, Cytomegalovirus and tumors: two players
662 for one goal-immune escape. *Open Virol. J* **5**, 60-69 (2011).
663 30. L. Vastag, E. Koyuncu, S. L. Grady, T. E. Shenk, J. D. Rabinowitz, Divergent effects of human
664 cytomegalovirus and herpes simplex virus-1 on cellular metabolism. *PLoS Pathog.* **7**, e1002124
665 (2011).
666 31. P. Kumari *et al.*, Essential role of HCMV deubiquitinase in promoting oncogenesis by targeting
667 anti-viral innate immune signaling pathways. *Cell Death Dis.* **8**, e3078 (2017).
668 32. D. Collins-McMillen *et al.*, Human Cytomegalovirus Promotes Survival of Infected Monocytes via
669 a Distinct Temporal Regulation of Cellular Bcl-2 Family Proteins. *J. Virol.* **90**, 2356-2371 (2015).
670 33. L. Soroceanu, C. S. Cobbs, Is HCMV a tumor promoter? *Virus Res.* **157**, 193-203 (2011).
671 34. B. Bhattacharjee, N. Renzette, T. F. Kowalik, Genetic analysis of cytomegalovirus in malignant
672 gliomas. *J. Virol.* **86**, 6815-6824 (2012).
673 35. M. El-Shinawi *et al.*, Human cytomegalovirus infection enhances NF-kappaB/p65 signaling in
674 inflammatory breast cancer patients. *PLoS One* **8**, e55755 (2013).
675 36. M. Michaelis *et al.*, Selection of a highly invasive neuroblastoma cell population through long-
676 term human cytomegalovirus infection. *Oncogenesis* **1**, e10 (2012).
677 37. P. Ranganathan, P. A. Clark, J. S. Kuo, M. S. Salamat, R. F. Kalejta, Significant association of
678 multiple human cytomegalovirus genomic Loci with glioblastoma multiforme samples. *J. Virol.*
679 **86**, 854-864 (2012).
680 38. L. Harkins *et al.*, Specific localisation of human cytomegalovirus nucleic acids and proteins in
681 human colorectal cancer. *Lancet* **360**, 1557-1563 (2002).
682 39. L. E. Harkins *et al.*, Detection of human cytomegalovirus in normal and neoplastic breast
683 epithelium. *Herpesviridae* **1**, 8 (2010).
684 40. J. Cinatl, M. Scholz, R. Kotchetkov, J. U. Vogel, H. W. Doerr, Molecular mechanisms of the
685 modulatory effects of HCMV infection in tumor cell biology. *Trends Mol. Med.* **10**, 19-23 (2004).
686 41. M. T. Nogalski *et al.*, A tumor-specific endogenous repetitive element is induced by
687 herpesviruses. *Nat. Commun.* **10**, 90 (2019).
688 42. E. Xiaofei, T. F. Kowalik, The DNA damage response induced by infection with human
689 cytomegalovirus and other viruses. *Viruses* **6**, 2155-2185 (2014).
690 43. X. E *et al.*, An E2F1-mediated DNA damage response contributes to the replication of human
691 cytomegalovirus. *PLoS Pathog.* **7**, e1001342 (2011).
692 44. D. J. Smart *et al.*, Assessment of DNA double-strand breaks and gammaH2AX induced by the
693 topoisomerase II poisons etoposide and mitoxantrone. *Mutat. Res.* **641**, 43-47 (2008).
694 45. K. Shimada *et al.*, TORC2 signaling pathway guarantees genome stability in the face of DNA
695 strand breaks. *Mol. Cell.* **51**, 829-839 (2013).
696 46. T. Waldman, K. W. Kinzler, B. Vogelstein, p21 is necessary for the p53-mediated G1 arrest in
697 human cancer cells. *Cancer Res.* **55**, 5187-5190 (1995).
698 47. M. Valverde *et al.*, Hydrogen Peroxide-Induced DNA Damage and Repair through the
699 Differentiation of Human Adipose-Derived Mesenchymal Stem Cells. *Stem Cells Int.* **2018**,
700 1615497 (2018).
701 48. B. Benedict *et al.*, Loss of p53 suppresses replication-stress-induced DNA breakage in G1/S
702 checkpoint deficient cells. *Elife* **7** (2018).
703 49. A. M. Schmitt *et al.*, An inducible long noncoding RNA amplifies DNA damage signaling. *Nat.*
704 *Genet.* **48**, 1370-1376 (2016).

705 50. L. F. Batista, B. Kaina, R. Meneghini, C. F. Menck, How DNA lesions are turned into powerful
706 killing structures: insights from UV-induced apoptosis. *Mutat. Res.* **681**, 197-208 (2009).
707 51. W. P. Roos, B. Kaina, DNA damage-induced cell death: from specific DNA lesions to the DNA
708 damage response and apoptosis. *Cancer Lett.* **332**, 237-248 (2013).
709 52. S. Liu *et al.*, Distinct roles for DNA-PK, ATM and ATR in RPA phosphorylation and checkpoint
710 activation in response to replication stress. *Nucleic Acids Res.* **40**, 10780-10794 (2012).
711 53. D. Woods, J. J. Turchi, Chemotherapy induced DNA damage response: convergence of drugs
712 and pathways. *Cancer Biol. Ther.* **14**, 379-389 (2013).
713 54. C. R. Hagan, R. F. Sheffield, C. M. Rudin, Human Alu element retrotransposition induced by
714 genotoxic stress. *Nat. Genet.* **35**, 219-220 (2003).
715 55. C. M. Rudin, C. B. Thompson, Transcriptional activation of short interspersed elements by DNA-
716 damaging agents. *Genes Chromosomes Cancer* **30**, 64-71 (2001).
717 56. A. Oberstein, T. Shenk, Cellular responses to human cytomegalovirus infection: Induction of a
718 mesenchymal-to-epithelial transition (MET) phenotype. *Proc. Natl. Acad. Sci. U.S.A.*
719 10.1073/pnas.1710799114 (2017).
720 57. A. Dobin *et al.*, STAR: ultrafast universal RNA-seq aligner. *Bioinformatics* **29**, 15-21 (2013).
721 58. A. Subramanian *et al.*, Gene set enrichment analysis: a knowledge-based approach for
722 interpreting genome-wide expression profiles. *Proc. Natl. Acad. Sci. U.S.A.* **102**, 15545-15550
723 (2005).
724 59. A. Liberzon *et al.*, The Molecular Signatures Database (MSigDB) hallmark gene set collection.
725 *Cell Syst.* **1**, 417-425 (2015).
726 60. J. M. Ford, M. B. Kastan, "11 - DNA Damage Response Pathways and Cancer" in Abeloff's
727 Clinical Oncology (Sixth Edition), J. E. Niederhuber, J. O. Armitage, M. B. Kastan, J. H.
728 Doroshow, J. E. Tepper, Eds. (Content Repository Only!, Philadelphia, 2020), pp. 154-
729 164.e154.
730 61. W. Lu, Y. Kang, Epithelial-Mesenchymal Plasticity in Cancer Progression and Metastasis. *Dev.*
731 *Cell* **49**, 361-374 (2019).
732 62. L. C. Kim, R. S. Cook, J. Chen, mTORC1 and mTORC2 in cancer and the tumor
733 microenvironment. *Oncogene* **36**, 2191-2201 (2017).
734 63. A. Hanna, L. A. Shevde, Hedgehog signaling: modulation of cancer properies and tumor
735 mircroenvironment. *Mol. Cancer* **15**, 24 (2016).
736 64. J. Falck, J. Coates, S. P. Jackson, Conserved modes of recruitment of ATM, ATR and DNA-
737 PKcs to sites of DNA damage. *Nature* **434**, 605-611 (2005).
738 65. G. Giglia-Mari, A. Zotter, W. Vermeulen, DNA damage response. *Cold Spring Harb. Perspect.*
739 *Biol.* **3**, a000745 (2011).
740 66. A. N. Blackford, S. P. Jackson, ATM, ATR, and DNA-PK: The Trinity at the Heart of the DNA
741 Damage Response. *Mol. Cell* **66**, 801-817 (2017).
742 67. J. Yuan, R. Adamski, J. Chen, Focus on histone variant H2AX: to be or not to be. *FEBS Lett.*
743 **584**, 3717-3724 (2010).
744 68. F. Delacote *et al.*, Chronic exposure to sublethal doses of radiation mimetic Zeocin selects for
745 clones deficient in homologous recombination. *Mutat. Res.* **615**, 125-133 (2007).
746 69. J. Smith, L. M. Tho, N. Xu, D. A. Gillespie, The ATM-Chk2 and ATR-Chk1 pathways in DNA
747 damage signaling and cancer. *Adv. Cancer Res.* **108**, 73-112 (2010).
748 70. Y. H. Ou, P. H. Chung, T. P. Sun, S. Y. Shieh, p53 C-terminal phosphorylation by CHK1 and
749 CHK2 participates in the regulation of DNA-damage-induced C-terminal acetylation. *Mol. Biol.*
750 *Cell* **16**, 1684-1695 (2005).
751 71. I. Hickson *et al.*, Identification and characterization of a novel and specific inhibitor of the ataxia-
752 telangiectasia mutated kinase ATM. *Cancer Res.* **64**, 9152-9159 (2004).
753 72. J. Greene *et al.*, The novel ATM inhibitor (AZ31) enhances antitumor activity in patient derived
754 xenografts that are resistant to irinotecan monotherapy. *Oncotarget* **8**, 110904-110913 (2017).
755 73. Y. Li, D. Q. Yang, The ATM inhibitor KU-55933 suppresses cell proliferation and induces
756 apoptosis by blocking Akt in cancer cells with overactivated Akt. *Mol. Cancer. Ther.* **9**, 113-125
757 (2010).

74. Y. Ziv *et al.*, Cellular and molecular characteristics of an immortalized ataxia-telangiectasia (group AB) cell line. *Cancer Res.* **49**, 2495-2501 (1989).
75. Y. Ziv *et al.*, Recombinant ATM protein complements the cellular A-T phenotype. *Oncogene* **15**, 159-167 (1997).
76. C. E. Canman *et al.*, Activation of the ATM kinase by ionizing radiation and phosphorylation of p53. *Science* **281**, 1677-1679 (1998).
77. A. Hirao *et al.*, DNA damage-induced activation of p53 by the checkpoint kinase Chk2. *Science* **287**, 1824-1827 (2000).
78. K. Cheung-Ong, G. Giaever, C. Nislow, DNA-damaging agents in cancer chemotherapy: serendipity and chemical biology. *Chem. Biol.* **20**, 648-659 (2013).
79. X. Dai, H. Cheng, Z. Bai, J. Li, Breast Cancer Cell Line Classification and Its Relevance with Breast Tumor Subtyping. *J. Cancer* **8**, 3131-3141 (2017).
80. S. Xu, X. Schafer, J. Munger, Expression of Oncogenic Alleles Induces Multiple Blocks to Human Cytomegalovirus Infection. *J. Virol.* **90**, 4346-4356 (2016).
81. Q. Lepiller, W. Abbas, A. Kumar, M. K. Tripathy, G. Herbein, HCMV activates the IL-6-JAK-STAT3 axis in HepG2 cells and primary human hepatocytes. *PLoS One* **8**, e59591 (2013).
82. C. R. Justus, N. Leffler, M. Ruiz-Echevarria, L. V. Yang, In vitro cell migration and invasion assays. *J. Vis. Exp.* 10.3791/51046 (2014).
83. Y. L. Liu *et al.*, Assessing metastatic potential of breast cancer cells based on EGFR dynamics. *Sci. Rep.* **9**, 3395 (2019).
84. A. V. Taubenberger, V. M. Quent, L. Thibaudeau, J. A. Clements, D. W. Hutmacher, Delineating breast cancer cell interactions with engineered bone microenvironments. *J. Bone Miner. Res.* **28**, 1399-1411 (2013).
85. C. C. Liang, A. Y. Park, J. L. Guan, In vitro scratch assay: a convenient and inexpensive method for analysis of cell migration in vitro. *Nat. Protoc.* **2**, 329-333 (2007).
86. G. M. Ehrenfeld *et al.*, Copper-dependent cleavage of DNA by bleomycin. *Biochemistry* **26**, 931-942 (1987).
87. Y. Pommier, E. Leo, H. Zhang, C. Marchand, DNA topoisomerases and their poisoning by anticancer and antibacterial drugs. *Chem. Biol.* **17**, 421-433 (2010).
88. M. T. Pickering, T. F. Kowalik, Rb inactivation leads to E2F1-mediated DNA double-strand break accumulation. *Oncogene* **25**, 746-755 (2006).
89. C. J. Bakkenist, M. B. Kastan, DNA damage activates ATM through intermolecular autophosphorylation and dimer dissociation. *Nature* **421**, 499-506 (2003).
90. A. Sarkar *et al.*, Ataxia telangiectasia mutated interacts with Parkin and induces mitophagy independent of kinase activity. Evidence from mantle cell lymphoma. *Haematologica* 10.3324/haematol.2019.234385 (2020).
91. P. Bouwman, J. Jonkers, The effects of deregulated DNA damage signalling on cancer chemotherapy response and resistance. *Nat. Rev. Cancer* **12**, 587-598 (2012).
92. F. G. Giancotti, Deregulation of cell signaling in cancer. *FEBS Lett.* **588**, 2558-2570 (2014).
93. L. Livraghi, J. E. Garber, PARP inhibitors in the management of breast cancer: current data and future prospects. *BMC Med.* **13**, 188 (2015).
94. B. Rodriguez-Martin *et al.*, Pan-cancer analysis of whole genomes identifies driver rearrangements promoted by LINE-1 retrotransposition. *Nat. Genet.* **52**, 306-319 (2020).
95. C. Cobbs, Cytomegalovirus is a tumor-associated virus: armed and dangerous. *Curr. Opin. Virol.* **39**, 49-59 (2019).
96. M. H. Luo, K. Rosenke, K. Czornak, E. A. Fortunato, Human cytomegalovirus disrupts both ataxia telangiectasia mutated protein (ATM)- and ATM-Rad3-related kinase-mediated DNA damage responses during lytic infection. *J. Virol.* **81**, 1934-1950 (2007).
97. R. M. Neve *et al.*, A collection of breast cancer cell lines for the study of functionally distinct cancer subtypes. *Cancer Cell* **10**, 515-527 (2006).
98. E. Murphy *et al.*, Coding potential of laboratory and clinical strains of human cytomegalovirus. *Proc. Natl. Acad. Sci. U.S.A.* **100**, 14976-14981 (2003).
99. K. Wu, A. Oberstein, W. Wang, T. Shenk, Role of PDGF receptor-alpha during human cytomegalovirus entry into fibroblasts. *Proc. Natl. Acad. Sci. U.S.A.* **115**, E9889-E9898 (2018).

100. E. Afgan *et al.*, The Galaxy platform for accessible, reproducible and collaborative biomedical analyses: 2018 update. *Nucleic Acids Res.* **46**, W537-W544 (2018).
101. Y. Liao, G. K. Smyth, W. Shi, featureCounts: an efficient general purpose program for assigning sequence reads to genomic features. *Bioinformatics* **30**, 923-930 (2014).
102. M. I. Love, W. Huber, S. Anders, Moderated estimation of fold change and dispersion for RNA-seq data with DESeq2. *Genome Biol.* **15**, 550 (2014).
103. Y. Liao, G. K. Smyth, W. Shi, The Subread aligner: fast, accurate and scalable read mapping by seed-and-vote. *Nucleic Acids Res.* **41**, e108 (2013).
104. A. F. A. Smit, R. Hubley, P. Green (2013-2015) RepeatMasker Open-4.0.
105. M. D. Robinson, A. Oshlack, A scaling normalization method for differential expression analysis of RNA-seq data. *Genome Biol.* **11**, R25 (2010).
106. H. Thorvaldsdottir, J. T. Robinson, J. P. Mesirov, Integrative Genomics Viewer (IGV): high-performance genomics data visualization and exploration. *Brief. Bioinform.* **14**, 178-192 (2013).
107. H. Heberle, G. V. Meirelles, F. R. da Silva, G. P. Telles, R. Minghim, InteractiVenn: a web-based tool for the analysis of sets through Venn diagrams. *BMC Bioinformatics* **16**, 169 (2015).
108. Y. Gao *et al.*, A double-negative feedback loop between E2F3b and miR- 200b regulates docetaxel chemosensitivity of human lung adenocarcinoma cells. *Oncotarget* **7**, 27613-27626 (2016).
109. H. H. Gari, G. D. DeGala, M. S. Lucia, J. R. Lambert, Loss of the oncogenic phosphatase PRL-3 promotes a TNF-R1 feedback loop that mediates triple-negative breast cancer growth. *Oncogenesis* **5**, e255 (2016).
110. K. J. Livak, T. D. Schmittgen, Analysis of relative gene expression data using real-time quantitative PCR and the 2(-Delta Delta C(T)) Method. *Methods* **25**, 402-408 (2001).
111. D. Rajapakse, K. Peterson, S. Mishra, G. Wistow, Serum starvation of ARPE-19 changes the cellular distribution of cholesterol and Fibulin3 in patterns reminiscent of age-related macular degeneration. *Exp. Cell. Res.* **361**, 333-341 (2017).
112. S. Upadhyay, S. Vaish, M. Dhiman, Hydrogen peroxide-induced oxidative stress and its impact on innate immune responses in lung carcinoma A549 cells. *Mol. Cell. Biochem.* **450**, 135-147 (2019).
113. S. Nakajima *et al.*, UV light-induced DNA damage and tolerance for the survival of nucleotide excision repair-deficient human cells. *J. Biol. Chem.* **279**, 46674-46677 (2004).
114. W. S. Rasband (1997-2010) ImageJ. (U.S. National Institutes of Health, Bethesda, Maryland, USA).

FIGURES

Figure 1.

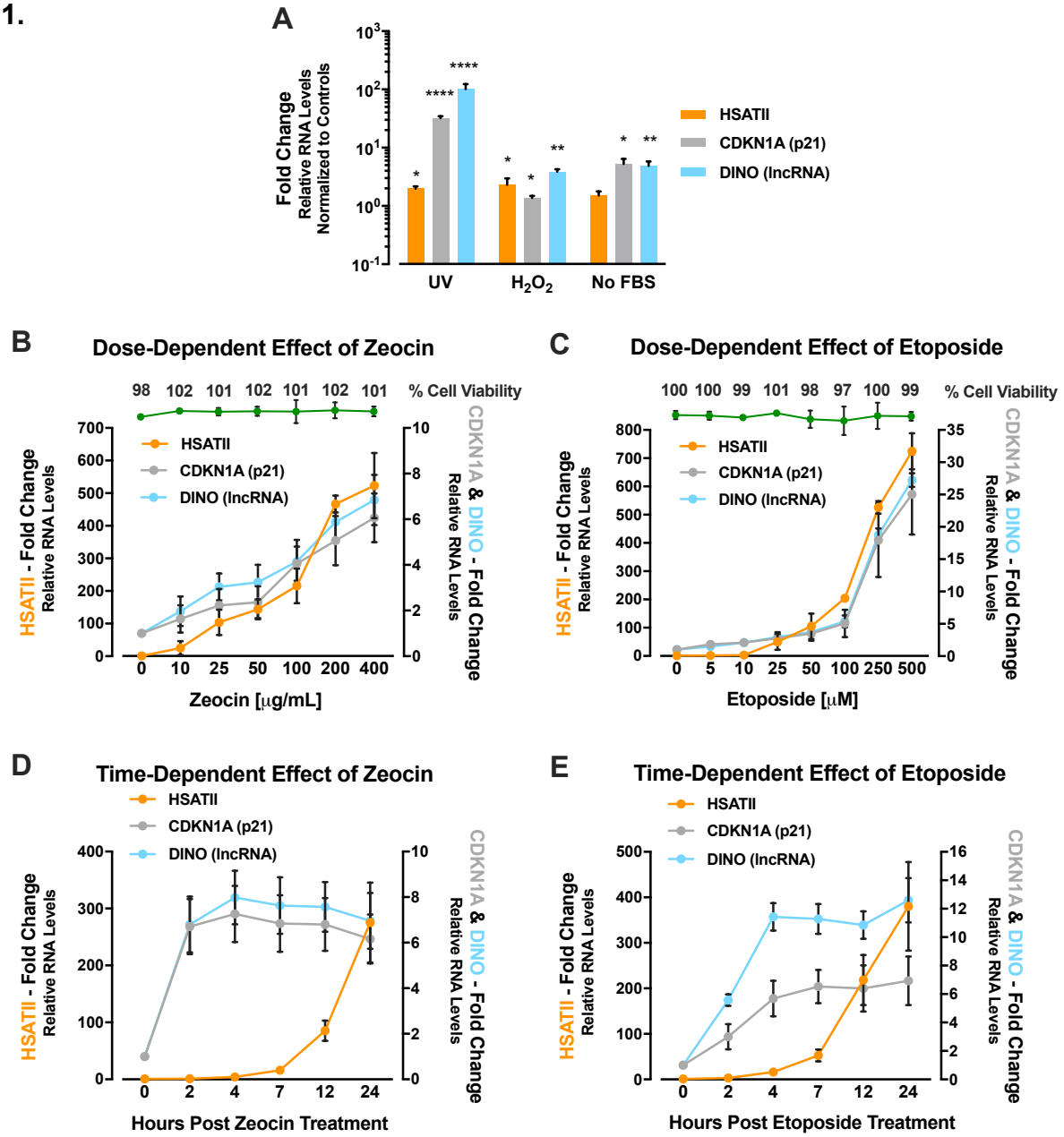

Fig. 1. DNA damage response regulates HSATII RNA expression. (*A*) Limited induction of HSATII RNA by UV, H_2O_2, or serum withdrawal. ARPE-19 cells were exposed to UV-irradiation (50 J/m^2), H_2O_2 (100 nM) or serum withdrawal (no FBS). RNA samples were collected at 24 hpt. RT-qPCR was performed to quantify HSATII, CDKN1A or DINO transcripts, using GAPDH as an internal control. Data are presented as a fold change (mean ± SD; n=3). **P*<0.05, ***P*<0.01, ****P*<0.001. (*B* and *C*) Induction of HSATII RNA by treatment with DNA-damaging drugs. ARPE-19 cells were treated with increasing concentrations of zeocin (*B*) or etoposide (*C*) with H_2O or DMSO, respectively, as solvent controls. RNA samples were collected at 24 hpt, and RT-qPCR was performed to quantify HSATII, CDKN1A and DINO transcripts, using GAPDH as an internal control. Data are presented as a fold change (mean ± SD; n=3). Insert: At 24 hpt, cell viability was assessed at each indicated drug concentrations. Data is presented as % viable cells, (mean ± SD; n = 3). (*D* and *E*) Drug-induced HSATII RNA accumulation occurs after a delay. ARPE-19 cells were treated with zeocin (200 μg/mL) (*D*), etoposide (200 μM) (*E*) and H_2O or DMSO, respectively, as solvent controls. RNA samples were collected at indicated times. RT-qPCR was performed to quantify HSATII, CDKN1A and DINO transcripts, using GAPDH as an internal control. Data are presented as a fold change (mean ± SD; n=3).

Figure 2.

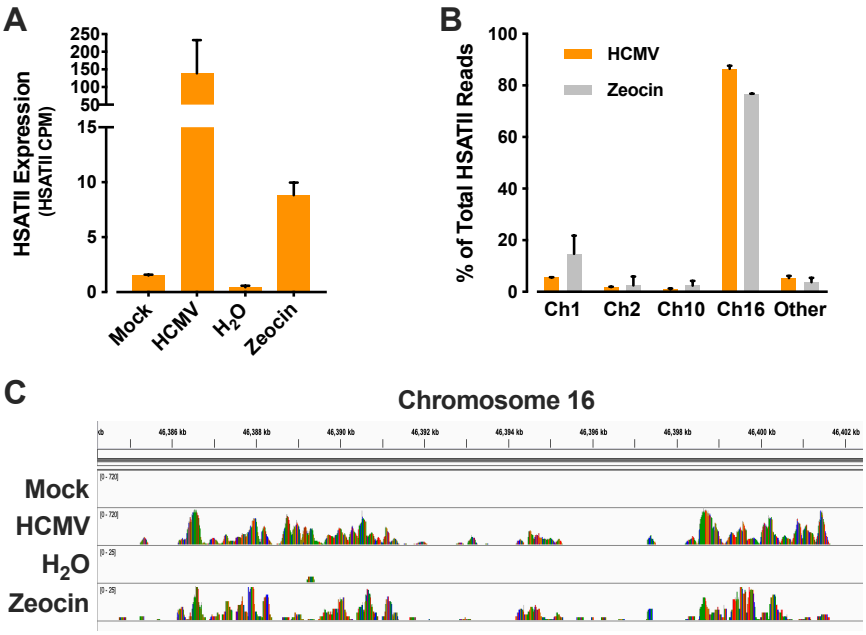

Fig. 2. Zeocin treatment partially mimics the transcriptional effect of HCMV infection on HSATII RNA expression. ARPE-19 cells were infected with HCMV (1 TCID50/cell), or treated with zeocin (100 μg/mL) or H_2O as a solvent control, and RNA samples were collected at either 24 hpi or 24 hpt, respectively. RNA was isolated and analyzed using RNA-seq. (*A*) Quantification of HSATII RNA induction by RNA-seq analysis. HSATII RNA expression in terms of counts per million reads mapped (CPM) was computed and normalized across samples (n=2). (*B*) Chromosomal distribution of HSATII RNA expression. HSATII chromosomal origin in HCMV-infected or zeocin-treated cells was depicted based on the number of unique HSATII reads mapped to specific chromosomal loci. Data are presented as a percentage of total HSATII reads (mean ± SD. n=2). (*C*) Example loci of HSATII RNA expression on chromosome 16. HSATII read coverage for HCMV-infection versus zeocin treatment was based on reads mapped to human genome and read coverage track at the HSATII locus on chromosome 16 was visualized using IGV.

937 **Figure 3.**

938
939
940
941
942
943

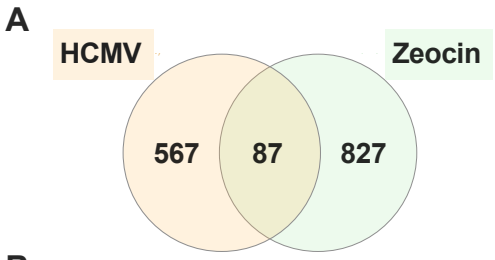

B

944
945
946
947
948

Gene Set Name	p-value	FDR q-value
HALLMARK_E2F_TARGETS	$2.64\ e^{-17}$	$1.32\ e^{-15}$
HALLMARK_G2M_CHECKPOINT	$3.31\ e^{-11}$	$8.26\ e^{-10}$
HALLMARK_EPITHELIAL_MESENCHYMAL_TRANSITION	$9.52\ e^{-5}$	$1.59\ e^{-3}$
HALLMARK_INTERFERON_GAMMA_RESPONSE	$1.13\ e^{-3}$	$1.13\ e^{-2}$
HALLMARK_MTORC1_SIGNALING	$1.13\ e^{-3}$	$1.13\ e^{-2}$
HALLMARK_HEDGEHOG_SIGNALING	$3.04\ e^{-3}$	$2.53\ e^{-2}$
HALLMARK_DNA_REPAIR	$4.87\ e^{-3}$	$3.48\ e^{-2}$
HALLMARK_APOPTOSIS	$5.92\ e^{-3}$	$3.7\ e^{-2}$

949

950 **Fig. 3.** Zeocin treatment partially mimics the HCMV-induced transcriptome. ARPE-19 cells were mock- or
951 TB40/E-GFP-epi-infected (1 $TCID_{50}$/cell), or treated with zeocin (100 μg/mL) or H_2O as a solvent control. After 24
952 h, RNA samples were collected, RNA was isolated and analyzed using RNA-seq. (*A*) Cellular genes modulated
953 by both HCMV and zeocin. Venn diagram showing significantly expressed genes ($q<0.05$) either in HCMV-
954 infected or zeocin-treated cells vs. respective controls. (*B*) Categories of gene sets modulated by both HCMV and
955 zeocin. GSEA was performed on the genes differentially expressed in both HCMV-infected and zeocin-treated
956 cells using the hallmark gene set of MSigDB. Identified specific gene set names are categorized based on
957 increasing *p*-value and FDR q-value.

958 **Figure 4.**

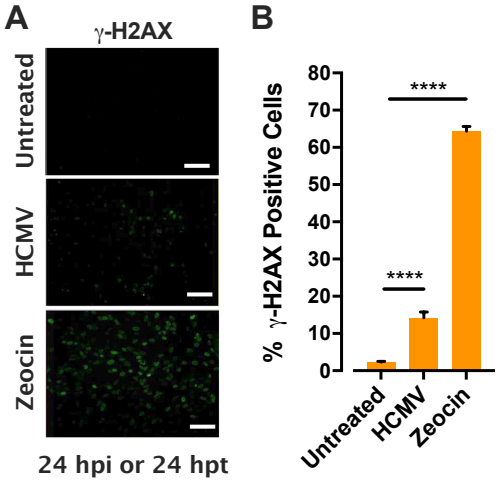

977 **Fig. 4.** HCMV and zeocin induce γ-H2AX in ARPE-19 cells. Cells were mock- or TB40/E-GFP-epi-infected (3
978 TCID50 /cell) or treated with zeocin (200 μg/mL). After 24 h, cells were stained for γ-H2AX, nuclei were
979 counterstained with the Hoechst stain, cells were visualized (*A*: scale bars=100 μm) and % γ-H2AX-positive cells
980 were quantified (*B*: mean ± SD; n=3). ****P<0.0001.

981

Figure 5.

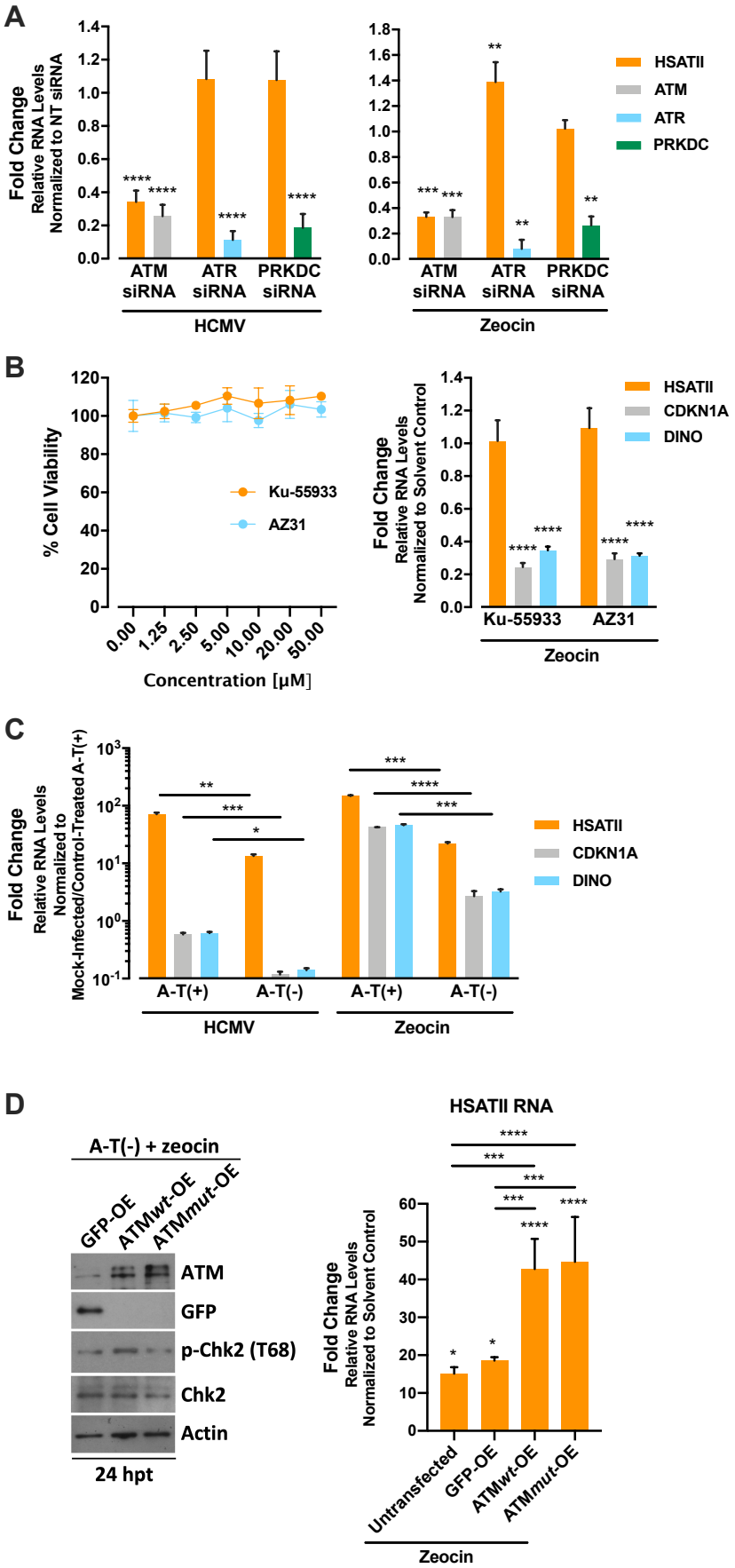
A
Fold Change
Relative RNA Levels
Normalized to NT siRNA
ATM siRNA
ATR siRNA
PRKDC siRNA
HCMV
Zeocin
HSATII
ATM
ATR
PRKDC
B
% Cell Viability
Ku-55933
AZ31
Concentration [μM]
Fold Change
Relative RNA Levels
Normalized to Solvent Control
HSATII
CDKN1A
DINO
C
Fold Change
Relative RNA Levels
Normalized to
Mock-Infected/Control-Treated A-T(+)
A-T(+)
A-T(-)
HCMV
Zeocin
D
A-T(-) + zeocin
GFP-OE
ATMwt-OE
ATMmut-OE
ATM
GFP
p-Chk2 (T68)
Chk2
Actin
24 hpt
HSATII RNA
Untransfected
Zeocin

1035
1036 **Fig. 5.** ATM-based DNA damage response regulates HSATII RNA expression. (*A*) ATM KD inhibits the induction
1037 of HSATII RNA by HCMV infection or zeocin treatment. ARPE-19 cells were transfected with ATM-, ATR- or
1038 PRKDC-specific siRNAs or NT siRNA as a control. After 48 h, cells were infected with TB40/E-GFP-epi (1
1039 $TCID_{50}$/cell) or zeocin (100 μg/mL). RNA samples were collected 24 h later. RT-qPCR was performed to quantify
1040 HSATII, ATM, ATR and PRKDC transcripts, using GAPDH as an internal control. Data are presented as a fold
1041 change (mean ± SD; n=3-10). (*B*) HSATII RNA is induced less in A-T(-) cells than in A-T(+). A-T(+) and A-T(-)
1042 cells were uninfected, infected with TB40/E-GFP (1 $TCID_{50}$/cell), or treated with zeocin (100 μg/mL) or H_2O as a
1043 solvent control. RNA samples were collected 24 h later. RT-qPCR was performed to quantify HSATII, CDKN1A
1044 and DINO transcripts, using GAPDH as an internal control. Data are presented as a fold change (mean ± SD;
1045 n=3). (*C*) ATM kinase inhibitors do not block the induction of HSATII RNA by zeocin. Left panel: ARPE-19 cells
1046 were treated with various concentrations of Ku-55933 or AZ31. At 24 hpt, cell viability was assessed. Data is
1047 presented as % viable cells, (mean ± SD; n=3). Right panel: ARPE-19 cells were treated with DMSO, Ku-55933
1048 (20 μM) or AZ31 (20 μM) for 2 h before zeocin (100 μg/mL) was added. RNA samples were collected 24 hpt, and
1049 RT-qPCR was performed to quantify HSATII, CDKN1A and DINO transcripts, using GAPDH was used as an
1050 internal control. Data are presented as a fold change (mean ± SD; n=3). (*D*) Ectopic expression of kinase-dead
1051 ATM (ATM*mut*) can enhance the induction of HSATII RNA in A-T(-) cells by zeocin. Left panel: A-T(-) cells were
1052 transfected with GFP-, ATM*wt*- or ATM*mut*-expressing plasmids. After 48 h, cells were exposed to zeocin (100
1053 μg/mL) and protein samples were collected 24 h later. Proteins were assayed by Western blot analysis performed
1054 using antibodies recognizing ATM, GFP, phospho-Chk2 (T68), Chk2 and actin as a loading control. Right panel:
1055 A-T(-) cells were transfected with GFP-, ATM*wt*- or ATM*mut*-expressing plasmids and untransfected cultures
1056 served as controls. After 48 h, cells were treated with zeocin (100 μg/mL) and RNA samples were collected 24 h
1057 later. RT-qPCR was performed to quantify HSATII. GAPDH was used as an internal control. Data are presented
1058 as a fold change (mean ± SD. n=4). *$P<0.05$, **$P<0.01$, ***$P<0.001$, ****$P<0.0001$.

1059 **Figure 6.**

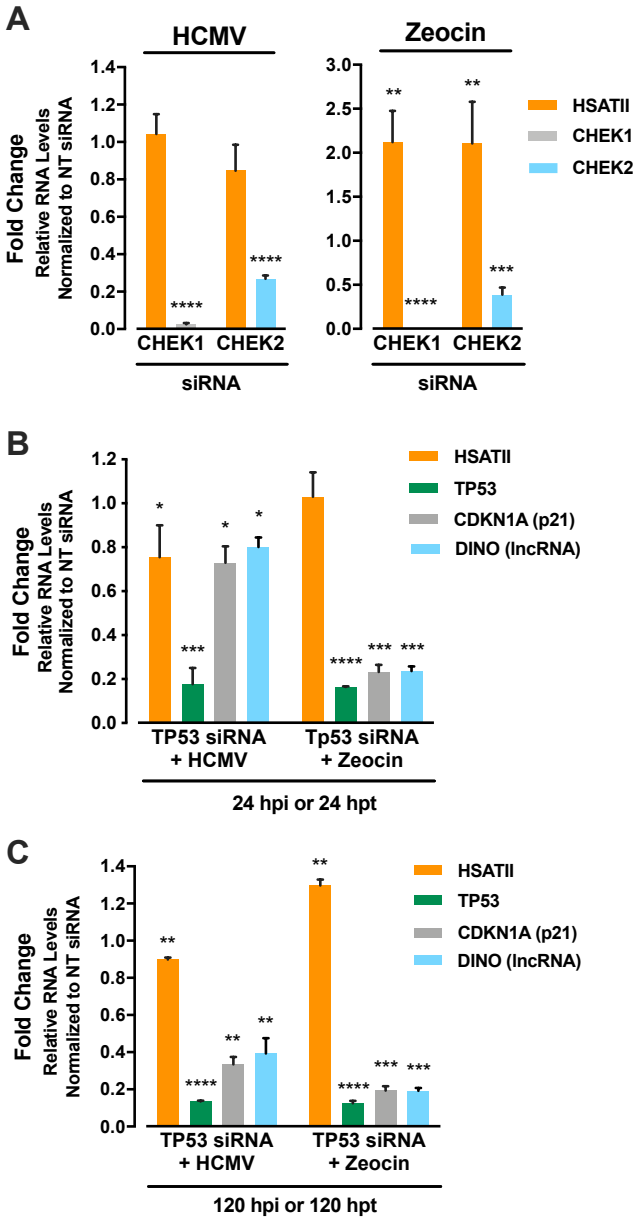

Fig. 6. HSATII RNA expression is induced via a Chk1/2- and p53-independent pathway. (*A*) CHEK1 or CHEK2 KD doesn't block HSATII RNA induction by infection or zeocin. ARPE-19 cells were transfected with CHEK1- or CHEK2-specific siRNA or NT siRNA as a control. After 48 h, cells were infected with TB40/E-GFP-epi (1 $TCID_{50}$/cell) or zeocin (100 μg/mL). RNA samples were collected 24 h later. RT-qPCR was performed to quantify HSATII, CHEK1 and CHEK2 transcripts, using GAPDH as an internal control. Data are presented as a fold change (mean ± SD; n=4). (*B* and *C*) p53 KD does not block HSATII RNA induction following HCMV infection or zeocin treatment. ARPE-19 cells were transfected with TP53 siRNAs or NT siRNA as a control. After 48 h, cells were infected with TB40/E-GFP-epi (1 TCID/cell) or zeocin (100 μg/mL), and RNA samples were collected 24 h (*B*) or 120 h (*C*) later. RT-qPCR was performed using specific primers to HSATII, TP53, CDKN1A or DINO transcripts. GAPDH was used as an internal control. Data are presented as a fold change (mean ± SD; n=3-4. **P*<0.05, ***P*<0.01, ****P*<0.001, *****P*<0.0001.

Figure 7.

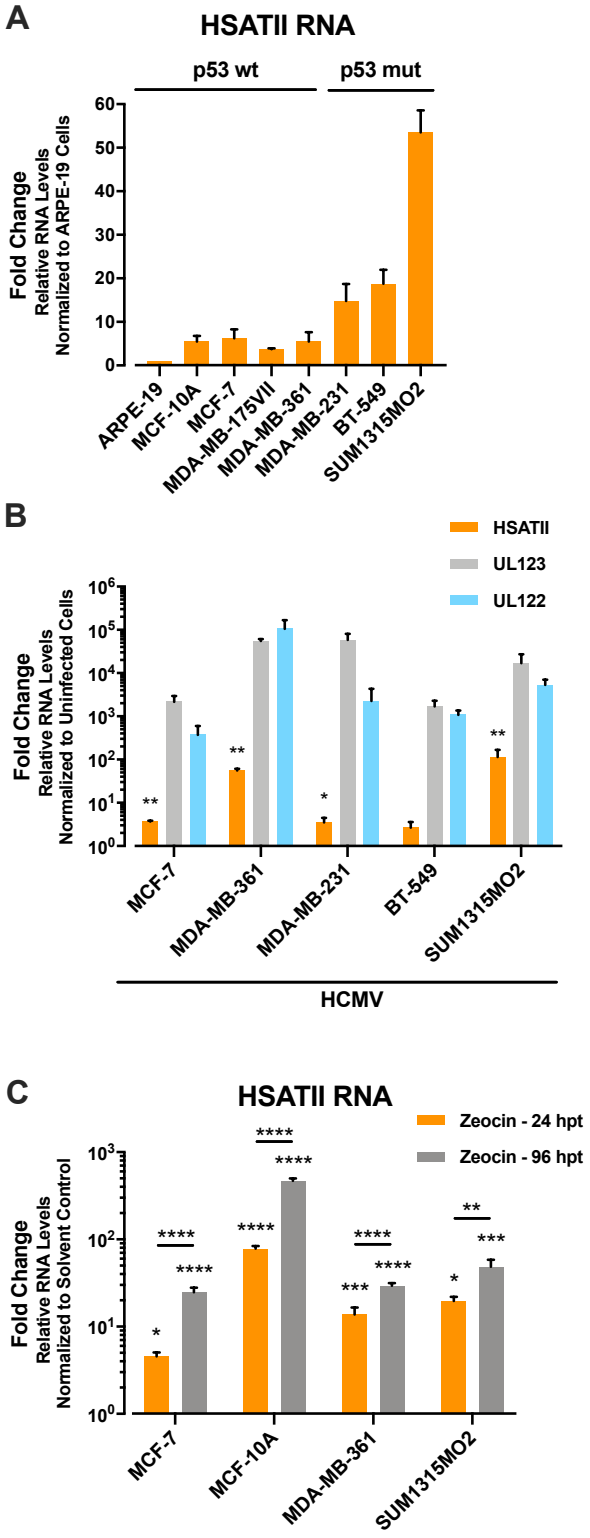

Fig. 7. Breast cancer cells differ in HSATII RNA levels and sensitivity to HCMV infection and zeocin treatment. (*A*) Breast cancer cell lines contain HSATII RNA when grown in adherent (2-dimensional) culture. Cell lines were grown to ~80% confluency and RNA samples were collected. RT-qPCR was performed to quantify HSATII RNA, using GAPDH as an internal control. Data are presented as a fold change (mean ± SD; n=3). (*B*) HCMV infection elevates HSATII RNA levels in breast cancer cell lines. MCF-7, MDA-MB-361, MDA-MB-231, BT-549 and SUM1315MO2 cells were infected with TB40/E-GFP-epi (4 $TCID_{50}$/cell) and RNA samples were collected at 24 hpi. RT-qPCR was performed to quantify HSATII RNA, using GAPDH as an internal control. Data are presented

1154 as a fold change (mean ± SD; n=3-5). (*C*) Zeocin treatment elevates HSATII RNA levels in breast cancer cell
1155 lines. MCF-7, MCF-10A, MDA-MB-361 and SUM1315MO2 cells were treated with zeocin (200 μg/mL). RNA
1156 samples were collected at 24 and 96 hpt and RT-qPCR was performed to quantify HSATII RNA, using GAPDH as
1157 an internal control. Data are presented as a fold change (mean ± SD; n=3). *P<0.05, **P<0.01, ***P<0.001,
1158 ****P<0.0001.

1159 **Figure 8.**

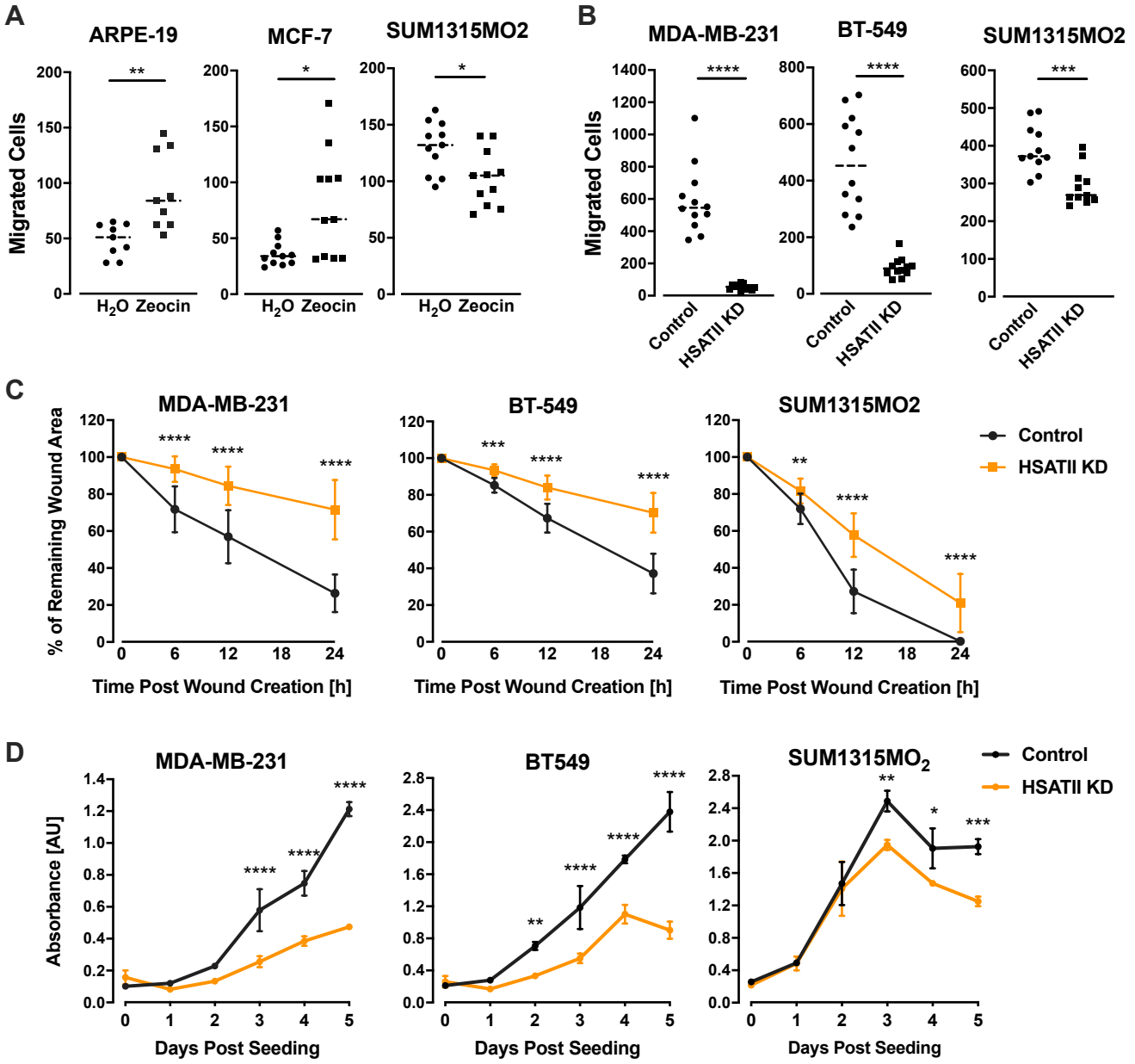

1160 **Fig. 8.** DNA damage-induced HSATII RNA enhances motility and proliferation of breast cancer cells. (*A*) Zeocin
1161 treatment increases migration of cells with low basal levels of HSATII RNA. ARPE-1, MCF-7 and SUM315MO2
1162 cells were treated with zeocin (200 μg/mL) for 24 h. Cells were transferred onto transwell inserts, and 24 h later,
1163 migrated cells were washed, fixed and nuclei stained. The graph presents a number of cells (with their indicated
1164 means) that migrated through a transwell per a field of view (FOV) from biological replicates. *n*=11. (*B*) Transwell
1165 assays demonstrated that HSATII KD reduces migration of breast cancer cells. MDA-MB-231, BT-549 and
1166 SUM1315MO2 cells were transfected with NT-LNA or HSATII-LNAs. After 48 hpt, equal number of cells was
1167 transferred onto transwell inserts. 24 h later, migrated cells were washed, fixed and nuclei stained. The graph
1168 presents a number of cells (with their indicated means) migrated through a transwell per FOV from biological
1169 replicates. n=12. (*C*) Wound-healing assays demonstrated that HSATII KD reduces migration of breast cancer
1170 cells. MDA-MB-231, BT-549 and SUM1315MO2 cells were transfected with NT-LNA or HSATII-LNAs. After 48

1171 hpt, wounds were created and their closure was monitored at indicated times. Data from biological replicates are
1172 presented as a percent of remaining wound width mean ± SD. n=20. (*D*) HSATII RNA KD reduces the rate of
1173 breast cancer cell proliferation in 2D culture. MDA-MB-231, BT-549 and SUM1315MO2 cells were transfected
1174 with NT-LNA or HSATII-LNAs. After 48 hpi, equal number of cells were seeded and cell proliferation was
1175 monitored at the indicated times. Cell proliferation is presented as an increase in a measured absorbance (AU –
1176 arbitrary units). n=3. *P<0.05, **P<0.01, ***P<0.001, ****P<0.0001.